W. W. Hansen Experimental Physics Laboratory
STANFORD UNIVERSITY
Stanford, California 94305-4085
Gravity Probe B Relativity Mission

S0672 Rev. –

March 27, 2003

Verification of T003 Telescope Bias and Scale-Factor Requirements

Prepared by

J. P. Turneaure, Robert P. Farley, John H. Goebel, & G. Mac Keiser

ITAR Assessment Performed
Tom Langenstein ______________ ITAR Control Required? Yes/No ______ Date 4.4.03

APPROVALS

		4/1/2003
G. Mac Keiser	GP-B Project Scientist	Date
		4/1/2003
John H. Goebel	Telescope Payload Subsystem	Date
		4/1/2003
Robert P. Farley	Telescope Readout Electronics	Date
		4/1/03
J.P. Turneaure	Telescope System	Date
		4/1/03
Barry Muhlfelder	Program Technical Manager	Date
		4/2/03
Anthony Logan	Systems Engineering	Date
		4/1/03
Dorrene Ross	Quality Assurance	Date

CHANGE RECORD

LIST OF ACRONYMS, ABBREVIATIONS AND SYMBOLS

α	Thermal expansion coefficient
β	Angle of sun with respect to the axis of the space vehicle. The angle is zero when the sun is facing the aft end of the space vehicle.
$\chi(\lambda,T)$	Photon absorption coefficient
$\pm\delta$	Fractional error or bias in $a^{+/-}$
δ_{FB}	Contribution to δ from the feedback capacitor temperature dependence
δ_{QE}	Contribution to δ from the photodetector quantum efficiency temperature dependence
γ_{FP}	Thickness of the telescope forward plate
γ_{PD}	Effective thickness of the layer in which photo conversion take place in the photodetectors
γ_W	Thickness of a window
η	Index of refraction
$d\eta/dT$	Temperature coefficient of the index of refraction
φ	Angle around an axis
κ	Thermal conductivity
λ	Wavelength of light
λ_0	Wavelength of the center of the 400 nm to 1000 nm optical band, which is 700 nm
μA	micro-ampere
μK	micro-kelvin
μm	micro-meter
μs	micro-second
μS	micro-siemen
μW	micro-watt
θ	True telescope pointing angle, angle between telescope axis and guide star
$\Delta\theta_b$	Total change in angular bias found in θ_m due to the complete telescope and telescope readout system
$\Delta\theta_{b,CE}$	Conditioning electronics contribution to $\Delta\theta_b$
$\Delta\theta_{b,FB}$	CCL feedback capacitor contribution to $\Delta\theta_b$
$\Delta\theta_{b,FP}$	Telescope forward plate contribution to $\Delta\theta_b$
$\Delta\theta_{b,MT}$	Telescope metering tube contribution to $\Delta\theta_b$
$\Delta\theta_{b,QE}$	Photodetector quantum efficiency contribution to $\Delta\theta_b$
$\Delta\theta_{b,R}$	Total telescope readout contribution of to $\Delta\theta_b$
$\Delta\theta_{b,T}$	Total telescope contribution to $\Delta\theta_b$
$\Delta\theta_{b,W}$	Contribution of windows to $\Delta\theta_b$
$\Delta\theta_{b,W3}$	Window #3 contribution to $\Delta\theta_b$
$\Delta\theta_{b,W4}$	Window #4 contribution to $\Delta\theta_b$
θ_m	Measured telescope pointing angle including errors and biases introduced by telescope system
$\Delta\phi_S$	Tilt angle change of the telescope secondary mirror axis with respect to the primary mirror axis
ρ	Radius in cylindrical coordinate system
σ	Linear scale factor for the change in photon flux with pointing angle at the roof prism for the plus and minus channels of the telescope readout
ξ_0	One-half of the photon flux of the image at the roof prism

$\xi^{+/-}$	Photon flux at the roof prism for the plus and minus channels of the telescope readout
Ω	ohm
ω_a	Annual angular frequency
ω_o	Orbital angular frequency
$a^{+/-}$	Calibration factors for plus and minus channels of the telescope readout that are used for forming S_n
ADC	Analog to Digital Converter
arcsec	arc-second
b	Scale factor that converts the normalized telescope pointing signal to angle
Δb	Small change in b
Δb_o	Component of Δb at orbital frequency
$\Delta b_{o,FP}$	Telescope forward plate contribution to Δb_o
$\Delta b_{o,MT}$	Telescope metering tube contribution to Δb_o
$\Delta b_{o,W3}$	Window #3 contribution to Δb_o
$\Delta b_{o,W4}$	Window #4 contribtuion to Δb_o
c	Velocity of light
C	degrees celsius
CLL	Charge Locked Loop
DAC	Digital to Analog Converter
d_i	Inside diameter of the telescope metering tube
d_o	Outside diameter of the telescope metering tube
d_w	Diameter across a window
DMA	Detector Mount Assembly
DPA	Detector Package Assembly
e-wave	extraordinary wave
EMI	Electromagnetic Interference
f	Focal length of telescope
FEE	Forward Equipment Enclosure

GP-B	Gravity Probe B
h	Planck's constant
Hz	hertz
$i^{+/-}$	Measured currents that are derived from the slope of the voltage ramps for the plus and minus channels of the telescope readout
JFET	J-type Field Effect Transistor
k	Boltzmann's constant
k_{FB}	Temperature coefficient of the fractional feedback capacitance in the charge locked loop
k_{QE}	Temperature coefficient of the fractional quantum efficiency
kΩ	kilo-ohm
K	kelvin
L	Length of metering tube
ΔL	Change in metering tube length
m	meter
marcsec	milli-arc-second
mg	milli-gram
milliarcsec	milli-arc-second
mK	milli-kelvin
mm	milli-meter
mW	milli-watt
Δn	Change in telescope defocus in the number of waves at a wavelength of 700 nm
Δn_ρ	Δn in radial direction
nm	nano-meter
nW	nano-watt
o-wave	ordinary wave
P	Heat power entering forward end of telescope
P_a	Component of P at annual frequency
$P_{T,FP}$	Transverse heat flow across diameter of telescope forward

	plate
$P_{T,MT}$	Transverse heat power flow around the telescope metering tube
pF	pico-farad
PID	Proportional-Integral-Differential
ppm	parts per million
pW	pico-watt
Q_c	Conversion efficiency of photons to electron-hole pairs
r_{FB}	Matching factor for the feedback capacitance temperature dependences between the plus and minus channels of a telescope readout
r_{QE}	Matching factor for the quantum efficiency temperature dependences between the plus and minus channels of a telescope readout
$R(\lambda)$	Reflection coefficient as a function of wavelength at the surface of the photodetector
R_{FP}	Radius of the telescope forward plate
R_{SM}	Spherical radius of the convex secondary mirror of the telescope
rad	radian
s	second
S_n	Normalized telescope pointing signal
SDTS	Si Diode Temperature Sensor
Si	Silicon
SiO	Silicon monoxide
SiO_x	Mixture of silicon monoxide and silicon dioxide
SI units	International system of units
SIA	Science Instrument Assembly
SQUID	Superconducting Quantum Interference Device

SRE	SQUID Readout Electronics
t	Time
T	Temperature
T_{FP}	Temperature of the telescope forward plate
ΔT_d	Temperature difference across a diameter
ΔT_{DMA}	Temperature change of the DMA platform
ΔT_{TRE}	Temperature change of the TRE
ΔT_ρ	Radial temperature difference in a window
$\Delta T_{\rho,a}$	ΔT_ρ at annual frequency
$\Delta T_{\rho,a,0}$	Amplitude of $\Delta T_{\rho,a}$
$\Delta T_{\rho,o}$	ΔT_ρ at orbital frequency
$\Delta T_{\rho,o,0}$	Amplitude of $\Delta T_{\rho,o}$
TRE	Telescope Readout Electronics
V	volt
$V^{+/-}$	Voltage at the output of the TRE analog electronics for the plus and minus channels
$dV^{+/-}/dt$	Derivative of the voltage ramps at the output of the charge locked loops for the plus and minus channels of the telescope readout
Ver.	Verification
W	watt
Δx_F	Position shift in the transverse position of the focal image relative to the telescope axis due to tilt angle change and transverse position change of the telescope secondary mirror
Δx_{FP}	Position shift in the transverse position of the telescope forward plate due to bending of the metering tube. This position shift is applicable to both the secondary mirror and the roof prisms.
yr	year

TABLE OF CONTENTS

LIST OF FIGURES

LIST OF TABLES

1 SUMMARY

The telescope system comprises the set of four windows, the telescope, the transport of the divided beams from the roof prism to the photodetectors, and the readout electronics. This document is an analysis of the angular bias variations and the scale-factor variations due to the telescope system. We find that the variations are dominated by those coming from the imaging system, namely the set of four windows and the telescope. For the telescope angular bias variation requirements, Table 1-1 lists the requirement paragraph number and title, the verification method, the required value, and the worst-case value found in this analysis document. The four sinusoidal variations in the table are given as angular amplitudes at their corresponding frequency. Table 1-2 lists the same information for the telescope scale-factor requirements with the percentage scale-factor variation at orbital frequency also given as an amplitude. Note that the percentage scale-factor variation at orbital frequency is treated as an amplitude in the verification of the T002 requirements. All seven requirements are met.

Table 1-1. Telescope system contribution to bias variation requirements and their verification

Requirement	Title	Ver. Method	Required Value	Worst-Case Value	Pass
7.6.2	Bias Variation	-	-	-	-
7.6.2.1	Linear Variation	A	< 0.1 marcsec/yr over 1 yr	0.058 marcsec/yr over 1 yr	Yes
7.6.2.2	Annual Variation	A	< 0.4 marcsec over 1 yr	0.029 marcsec over 1 yr	Yes
7.6.2.3	Orbital Variation	A	< 0.1 marcsec over 1 yr	0.029 marcsec over 1 yr	Yes
7.6.2.4	Linear Drift	A	< 1000 marcsec/yr over 1 yr	51 marcsec/yr over 1 yr	Yes
7.6.2.5	Bias Variation at Other Frequencies	A	< 1000 marcsec over 1 yr	7.4 marcsec over 1 yr	Yes

The worst-case values in Table 1-1 and Table 1-2 are dominated by the temperature variations of Window #3, Window #4, and the telescope. We expect that these worst-case values will be reduced substantially when the actual temperature history for these items are available from the flight data. We had to make very conservative estimates of the temperature coefficients of the index of refraction for fused quartz and sapphire because of the lack of a good database for these materials. Additional measurements of the temperature coefficients of the index of refraction for the fused quartz and sapphire material used in the flight build at the actual temperatures of the windows and telescope would allow the worst-case values to be reduced even further.

Table 1-2. Telescope system contribution to scale-factor variation requirements and their verification

Requirement	Title	Ver. Method	Required Value	Worst-Case Value	Pass
7.6.3	Small Angle Scale Factor Variation	-	-	-	-
7.6.3.1	Orbital Frequency Scale Factor Variation	A	< 2 % (amplitude) over 1 week	0.49 % (amplitude) over 1 week	Yes
7.6.3.2	Linear Drift in Telescope Scale Factor	A	< 2 %/day over 1 day	0.07 %/day over 1 day	Yes

2 INTRODUCTION

This analysis document provides the verification of the T003 telescope bias variation and small angle scale-factor variation requirements. These requirements are listed in section 2.1. Section 3 provides a description of the telescope system. Section 4 contains the detailed analyses that verify the requirements.

2.1 T003 Requirements

7.6.2 Bias Variation

The variation in the bias of the telescope normalized pointing signal (including the effects from the telescope, the telescope electronics, and the A/D sampling) has the following requirements:

Verification Method: **N/A**

7.6.2.1 Linear Variation

The amplitude of any linear variation in the body-fixed bias signal at roll frequency (linear variation in the inertially-fixed bias) and the body-fixed SQUID calibration signal frequency shall be less than 0.1 marcsec for data taken over the course of one year during the time the guide star is valid.

Verification Method: **A**

7.6.2.2 Annual Variation

The amplitude of any variation at annual rate in the body-fixed bias at roll frequency (annual variation in the inertially-fixed bias) and the body-fixed SQUID calibration signal frequency shall be less than 0.4 marcsec for data taken over the course of one year during the time the guide star is valid.

Verification Method: **A**

7.6.2.3 Orbital Variation

The amplitude of any variation at orbital rate in the body-fixed bias signal at roll frequency (orbital variation in the inertially-fixed bias) and the body-fixed SQUID calibration signal frequency shall be less than 0.1 marcsec for data taken over the course of one year during the time the guide star is valid.

Verification Method: **A**

7.6.2.4 Linear Drift

The linear drift in the body-fixed bias shall be less than 1,000 milliarcseconds in one year for data taken over the course of one year during the time the guide star is valid.

Verification Method: **A**

7.6.2.5 Bias Variations at Other Frequencies

The amplitude of a body-fixed signal at any other frequency not covered in the above requirements shall be less than 1,000 milliarcsec for data taken over the course of one year during the time the guide star is valid.

Verification Method: **A**

7.6.3 Small Angle Scale Factor Variation

The telescope scale factor variation during guide star valid meets the following requirements:

Verification Method: **N/A**

7.6.3.1 Orbital Frequency Scale Factor Variation

The variation in the small angle telescope scale factor at orbital frequency averaged over one week shall be less than 2 %.

Verification Method: **A**

7.6.3.2 Linear Drift in Telescope Scale Factor

The linear drift in the small angle telescope scale factor shall be less than 2 % over any one day period.

Verification Method: **A**

3 DESCRIPTION OF THE TELESCOPE SYSTEM

The telescope system includes the window subsystem, the telescope optics, the transport and analog readout of the optical beams split by the two roof prisms, and the analog to digital conversion of these signals.

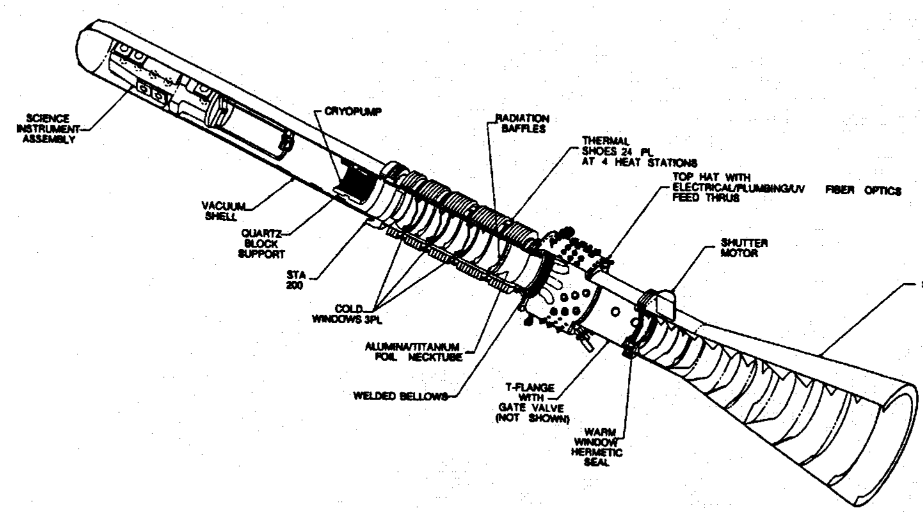

Figure 3-1. Low-temperature vacuum probe

3.1 Window Subsystem

The window subsystem comprises four windows in series, which are all manufactured to produce little distortion of the guide star wavefront. Figure 3-1 is a simplified drawing of the flight probe showing the location of the four windows. The outer window, Window #4, labeled as "Warm Window Hermetic Seal" in Fig. 3-1 acts as a vacuum seal for the probe. The inner three windows, Window #1 through Window #3, labeled as "Cold Windows 3 Pl" in Fig. 3-1 are located at various heat stations within the probe vacuum and act to reduce thermal radiation reaching the science instrument and to reduce the parasitic heat loss to the dewar. The predicted temperatures of the four windows [Burns 2002] are listed in Table 3-1. Each window is canted at a slight angle to avoid having ghost images of the guide star within the field of view of the telescope due to multiple reflections. The transmission coefficient of the window subsystem as a function of wavelength was measured by Lockheed Martin.

Table 3-1. Predicted on-orbit temperatures for windows

Window	Predicted on-orbit temperature
#1	28 K
#2	72 K
#3	129 K
#4	238 K

Table 3-2. Properties of Window #4

Property	Value	Reference
Thickness	0.275 inch	[Lockheed 1995]
Diameter	8.000 inch	[Lockheed 1995]
Index of Refraction @ 296 K for 707 nm	1.763 (o-wave) 1.755 (e-wave)	[Malitson 1962], [Burch 1965]
Index of Refraction at 296 K for 3.39 μm	1.699 (o-wave) 1.692 (e-wave)	[Yang 2001]
Temperature Coefficient of the Index of Refraction @ 296 K for 3.39 μm	1.14×10^{-5} /K (o-wave) 1.28×10^{-5} /K (e-wave)	[Yang 2001]
Thermal Expansion Coefficient	8.4×10^{-6} /K	Crystal Systems Brochure

The temperature of Window #4 is about the same as that of the outer ambient temperature of the space vehicle. The window is a 0.275 inch thick single crystal sapphire window with its A-axis parallel to the probe axis [Lockheed 1995]. Window #4 also has a conductive coating that serves as a Faraday shield and as an EMI filter. This conductive coating is electrically in contact with the probe around the periphery of Window #4. Some of the properties of this window are given in Table 3-2. We found data at room temperature for the temperature coefficient of the index of refraction [Yang 2001] $d\eta/dT$ only at a wavelength of 3.39 μm rather than at 700 nm (700nm is in the middle of the 400 nm to 1000 nm band, which contains most of the useful spectrum from the guide star). To be conservative, we use twice the value at 3.39 μm in the later analyses.

As seen in Table 3-1, Window #1 through Window #3 are at successively higher temperatures. They are made from a high quality optical grade of fused quartz called Herasil®†. These windows are 0.650 inch thick and are anti-reflection coated [Lockheed 1996]. Some of the properties of these windows are given in Table 3-3. We only found data for the temperature coefficient of the index of refraction $d\eta/dT$ at room temperature. As seen in Table 3-1, the fused-quartz windows are in fact substantially below room temperature. The data for various optical glasses [D'Ans 1962] suggest that the room temperature value of $d\eta/dT$ for fused quartz is satisfactory as a worst-case value for temperatures below room temperature.

Table 3-3. Properties of fused-quartz windows

Property	Value	Reference
Thickness	0.650 inch	[Lockheed 1996]
Diameter	6.500 inch	[Lockheed 1996]
Index of Refraction at 292 K for 700 nm	1.455	Heraeus-Amersil Brochure 40-1015-079
Temperature Coefficient of the Index of Refraction at 292 K for 644 nm	9.7×10^{-6} /K	Heraeus-Amersil Brochure 40-1015-079
Thermal Expansion Coefficient at 292 K	4.0×10^{-7} /K	Heraeus-Amersil Brochure 40-1015-079

3.2 Telescope Optics

Figure 3-2 is a simplified drawing of the Gravity Probe B (GP-B) star tracking telescope. The telescope is a reflecting type telescope with all of its structural components made from Herasil®† fused quartz. As seen in Fig. 3-1, the telescope is mounted to a fused-quartz block, also made from Herasil®† fused quartz. The entire fused quartz assembly containing the telescope and four gyroscopes is called the Science Instrument Assembly (SIA). On orbit during science data taking operations, the SIA is at a temperature of less than 5 K, with the fused quartz block at about 2.5 K and the forward plate of the telescope at about 5 K. Scale-factor and bias variations require knowledge of the temperature

† Herasil® is a product of Heraeus-Amersil.

coefficient of the index of refraction of the telescope front plate, which is at about 5 K. Data for $d\eta/dT$ around 5 K for Suprasil-W®† (a form of pure fused quartz) [Phillips 1981] indicate that the room temperature value for fused quartz in Table 3-3 is a satisfactory worst-case value.

To form an image the telescope has three mirrors: a primary mirror, which is concave, a secondary mirror, which is convex, and a tertiary mirror, which is also convex. This combination of mirrors yields a focal length of 3.566 m even though the overall physical length of the telescope is only about 0.35 m. The guide star wavefront enters the telescope through an annular region of the optically flat forward plate from the upper right in Fig. 3-2. It is then successively reflected from the primary, secondary, and tertiary mirrors to form an image within the image divider assembly located on the forward plate (labeled corrector plate in Fig. 3-2). The secondary and tertiary mirrors are convex spherical mirrors, and the primary mirror is an aspheric concave mirror to correct for spherical aberration. The geometrical properties of the fused-quartz telescope elements are listed in Table 3-4.

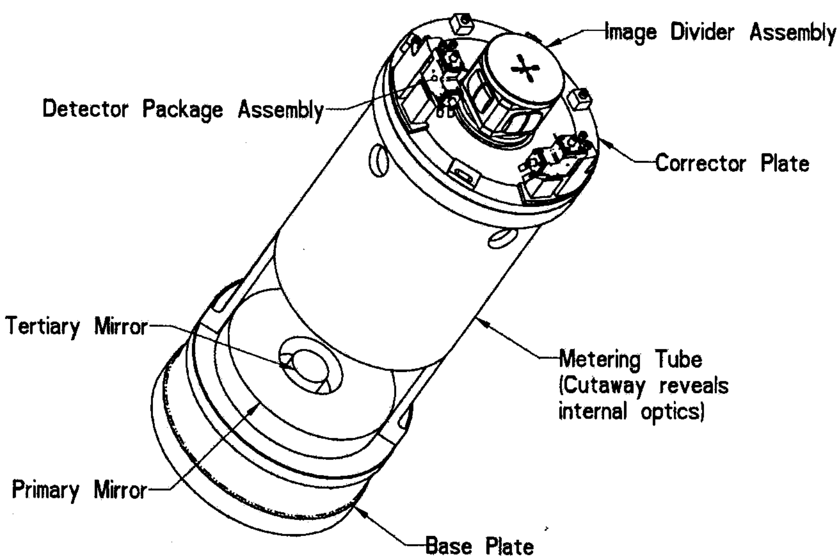

Figure 3-2. Simplified drawing of the flight telescope

Figure 3-3 is a schematic diagram of the roof prism for a single axis and the transport of the divided beams to the redundant pairs of photodetectors. Located in the optical path in front of the roof prisms, there is an aperture stop to limit the telescope field of view to less than 90 arcsec (see Fig. 3-3). Within the image divider assembly there is a beam splitter so that there are two images, each falling on its own roof prism (see Fig. 3-3). The roof prisms are oriented in such a way that one splits the image to find the image centroid for one of the telescope axes, and the second one splits the image to find the image centroid for the other axis.

---

† Suprasil-W is a product of Heraeus-Amersil.

Table 3-4. Properties of the fused-quartz telescope elements

Element	Property	Value	Reference
Primary Mirror	Spherical Radius (concave)	47.477 inch	SUGPB Dwg 25081 C
Secondary Mirror	Spherical Radius (convex)	91.202 inch	SUGPB Dwg 25079 D
	Inside Diameter of Clear Aperture	2.795 inch	
Tertiary Mirror	Spherical Radius (convex)	7.484 inch	SUGPB Dwg 25080 C
Metering Tube	Length	13.66 inch	SUGPB Dwg 25061 D
	Outside Diameter	6.500 inch	
	Inside Diameter	5.900 inch	
Forward Plate	Diameter	7.250 inch	SUGPB Dwg 25060 F
	Thickness	0.400 inch	
	Outside Diameter of Clear Aperture	5.660 inch	

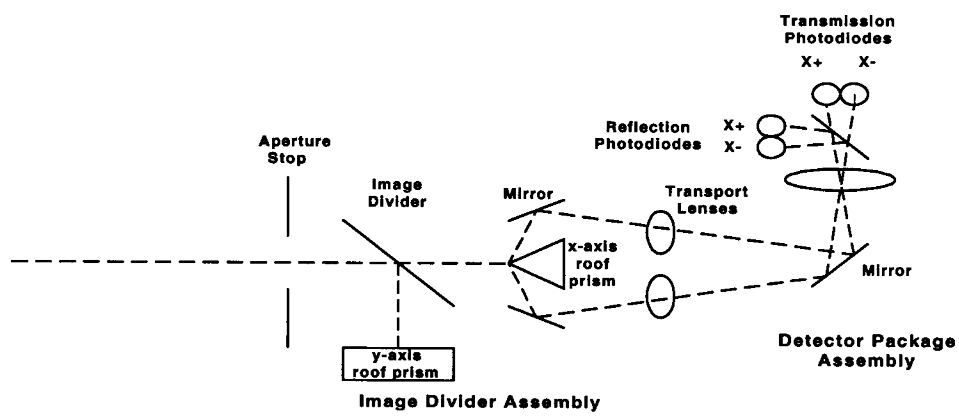

Figure 3-3. Schematic of roof prism and transport of divided beams

3.3 Transport of Divided Beams

As stated in the previous section, Fig. 3-3 depicts the transport of the divided beams from the roof prism to the redundant pairs of photodetectors. For each axis, the image is divided by its roof prism, which has an aluminum reflective coating. The resulting divided beams for each telescope axis, called the plus and minus beams, are transported by a series of mirrors and lenses to the photodetector pairs within the Detector Package Assemblies (DPAs). Each DPA, which is located on the forward plate of the telescope, serves one of the telescope axes. Within each DPA there is a beam splitter that allows the divided beams to fall on the redundant pairs of photodetectors: the photodetector pair for the transmitted beams, and the photodetector pair for the reflected beams. The two photodetectors of each photodetector pair are labeled as the plus photodetector associated with one side of the divided beams and the minus photodetector associated with the other side. The transport optics system is a tradeoff between providing a good focus of the divided beams on the photodetectors and minimizing the steering of the image on the photodetectors with the telescope pointing angle. The photodetectors are the interface between the optical and electronic subsystems.

3.4 Analog Electronics

Figure 3-4 is a schematic drawing of the analog electronics for the readout of a single photodetector. The vertical line in the figure shows the division of the electronics between the portion mounted on the detector mount assembly (DMA), which is located in the DPA, and the portion located in the telescope readout electronics box (TRE), which is located within the forward equipment enclosure (FEE) of the space vehicle. Each DMA has two such electronic circuits, one each for the plus and the minus photodetectors. Each DPA contains two DMAs, called the primary and redundant channels. Finally, the telescope has two DPAs, one for reading out each of the two telescope axes. The analog electronics has two sections, the charge locked loop (CLL), which integrates the photodetector current, and the conditioning electronics. The CLL and conditioning electronics are sensitive to temperature variations of the DMA platforms and the TRE boxes. For this reason, the temperature variations of the TRE boxes and DMA platforms are analyzed in sections 3.7 and 3.8.

3.4.1 Charge Locked Loop

The two DPAs are mounted directly on the telescope forward plate, and they are thus thermally sunk to the temperature of the forward plate, which is about 5 K during science data taking. The photodetectors and the preamplifier electronics for the CLL are located on a thermally isolated single-crystal sapphire platform. The sapphire platform and the electronic circuits on it comprise a DMA. The sapphire platform is heated by the power dissipated in the preamplifiers and in a heater. We set the temperature of the sapphire platform to 72 K, which is within the temperature region where the photodetectors and JFET preamplifiers perform optimally. The JFET differential preamplifier design compensates for temperature sensitivities of the components by using closely matched components. This analog electronic circuit is a charge locked loop that integrates the photocurrent on a 0.59 pF feedback capacitor (indicated as 0.5 pF in Fig. 3-4). The transimpedance of the JFETs is 316 μS. Using this value and the circuit diagram in Fig. 3-4, the charge locked loop voltage error amplifier has a voltage gain of 69,000. This voltage gain is quite stable since the JFET stages are on the temperature stabilized DMA platforms at low temperature and the two gain stages in the TRE use low temperature coefficient feedback resistors. The output of the charge locked loop is a voltage ramp, whose slope is proportional to the photocurrent. The feedback capacitor is the element that determines the scale factor for converting the slope of the voltage ramp to photocurrent. The voltage ramp is reset at a 10 Hz rate so the effective ramp period is just under 0.1 s when allowing for the settling time after a reset.

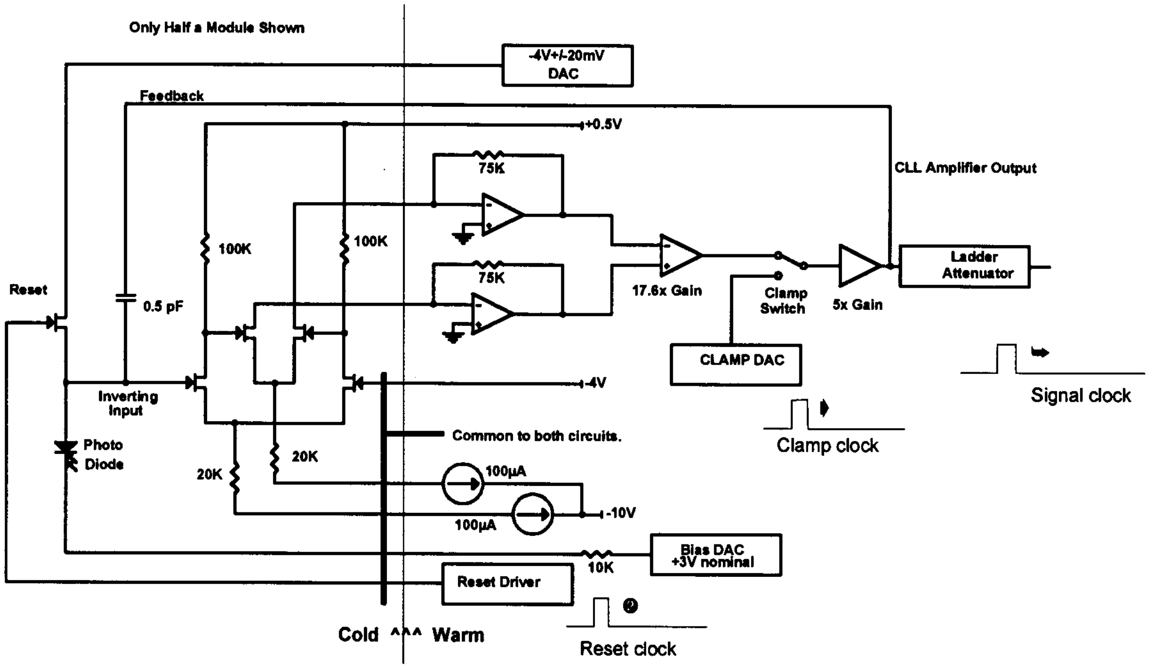

Figure 3-4. Schematic of analog electronics

3.4.2 Conditioning Electronics

The analog conditioning electronics have a commandable voltage gain, indicated in Fig. 3-4 by the ladder attenuator block, so that the output can be set to span at least ¼ of the 16 bit analog-to-digital converter (ADC) range. It consists of a digitally commanded analog attenuator, and three voltage amplifier stages with a total gain of 2552.

3.5 Digital Electronics

The conditioned analog outputs of the voltage ramps are conducted to the SQUID Readout Electronics box (SRE), which is located within the FEE. The voltage ramps are converted to digital signals within the SRE using a 16 bit ADC. The ADC has a linearity of ±½ bit, and it has a high quality, low temperature sensitivity voltage reference. The voltage reference is mounted on a temperature regulated printed wire board. Using a multiplexer, the same ADC is used for readout of the voltage ramps for both the plus and minus sides of a photodetector pair with the result that differential gain drifts are negligible. The voltage ramps are digitally sampled at 2200 Hz.

3.6 Digital Signal Processing

The voltage ramps are processed in two ways to estimate the pointing angles. For attitude control of the space vehicle, the voltage ramps are processed to find the photocurrents using a simpler algorithm that requires less processing time by the on-board computers. For science analysis, the photocurrents are estimated using a Kalman filter to minimize the error of the photocurrent estimates. The normalized telescope pointing signal S_n, which is independent of the guide star irradiance, is derived from the plus and minus photocurrents and the measured relative efficiencies of the plus and minus channels of the telescope readout (see section 4.2). The absolute telescope pointing angles are found by multiplying the normalized telescope pointing signals by a scale factor b, which depends on the telescope focal length and image quality and which is accurately determined using scale-factor matching. The signal processing does not introduce any significant contributions to the bias and scale-factor variations since the data is processed digitally with adequate precision.

3.7 Temperature Variations of TRE and SRE

The A-side and B-side TRE boxes and SRE forward boxes, which contain circuit elements that are temperature sensitive, are located in the FEE. The A-side TRE box and A-side forward SRE box are in physical and thermal contact with each other at one axial angle, and likewise for the B-side TRE box and B-side forward SRE box at another axial angle. Table 3-5 lists the temperature amplitudes determined by analysis [Burns 1998] of these boxes at roll frequency, orbital frequency, and annual frequency. A maximum linear drift is found with a linear least squares fit of a linear drift term over one year to the annual variation assuming the initial phase of the sine wave that gives the largest drift value. It is useful to note that, for roll frequency, the sensitive components within these boxes have temperature variations less than or equal to the values in the table due to both passive thermal filtering and active temperature control of some printed wire boards. In the following analyses, we use the temperature variation of the TREs as representative because the most critical temperature sensitive components in the telescope readout electronics are in the TRE and because the forward SRE temperature variations are only slightly different from those of the TRE.

Table 3-5. Temperature stability of TRE boxes and SRE forward boxes

Property	Box Temperature Variation			
	A-Side		B-Side	
	TRE	SRE	TRE	SRE
Amplitude at Roll Frequency	0.0065 K	0.005 K	0.0105 K	0.0075 K
Amplitude at Orbital Frequency	0.12 K	0.135 K	0.12 K	0.14 K
Amplitude at Annual Frequency	8.7 K	8.85 K	7.5 K	7.6 K
Linear Drift	4.2 K/yr	4.2 K/yr	3.6 K/yr	3.6 K/yr

3.8 Temperature Stability of DMA

The heat power for each DMA, when it is at 72 K, is 0.80 mW, with 0.66 mW coming from the current bias of the JFET preamplifiers and 0.14 mW dissipated in a heater resistor on the DMA, which can be used for temperature control [Farley 2001a]. The temperature of the DMA is sensed with a silicon diode temperature sensor (STDS), which is biased with a 10 μA current source. The voltage across the STDS is a measure of the DMA temperature. There are two modes that can be used for control of the temperature: a passive mode and a proportional-integral-differential (PID) mode. There is also a third mode that is not used because it introduces excessive noise into the photodetector current readout.

3.8.1 Passive Mode

In the passive mode, the DMA temperature of 72 K is determined from the power dissipated by the JFET preamplifiers from their constant bias currents and the constant power dissipation in the heater resistor. In this mode, the DMA temperature stability is in part affected by the temperature control of the quartz block, which controls the quartz block flange temperature with a temperature stability of less than 1 mK rms [Muhlfelder 2001]. The telescope forward plate is at about 5 K due to the heat dissipation from the DMAs and thermal radiation down the probe. The thermal time constant of the telescope forward plate relative to the quartz block flange is large compared to roll period, and thus there is substantial passive filtering of the temperature variations at the quartz block flange at roll frequency. A simple estimate yields a filter factor of at least 20 at roll frequency. Further the DMA temperature variation due to the quartz block flange temperature variation is further reduced by the increasing thermal conductivity with increasing temperature. Thus in this passive mode as we find below, the DMA temperature variation is dominated by the variation of the current biases for the JFET preamplifiers and the power dissipated in the heater resistors.

Farley [Farley 2003b] measured the temperature coefficient of the current bias to a JFET preamplifier of 0.160 μA/K [TRE] during the box level thermal vacuum testing of the TRE boxes. The total power dissipated by the 100 μA bias for the 8 preamplifier circuits is 2.64 mW. Thus, assuming a worst-case resistive load, the temperature coefficient of power dissipation is 8.45 μW/K [TRE].

Each heater resistor is powered with a Harris-565ARH-8 DAC (part # 5962R9675501VJC) operated in its unipolar mode, which has a worst-case temperature coefficient of voltage output of 2 ppm/K [Harris 1994]. The total dissipated power for all four heater resistors is 0.56 mW, and thus the temperature coefficient of power dissipation is 2 nW/K [TRE], which is clearly negligible compared with that from the temperature coefficient of the constant current bias.

The total temperature coefficient of power dissipation is 8.45 μW/K [TRE], which is dominated by variations in the power dissipated in the JFET preamplifiers. We now estimate the TRE temperature coefficient of DMA temperature using the fact that the total power dissipated in all four DMAs is 3.2 mW and the temperature drop through the DMA thermal isolators is 67 K, which yields an average value of thermal conduction of 47.8

μW/K. Combining this value with the temperature coefficient of power dissipation yields a temperature coefficient of 177 mK [DMA]/K [TRE]. Table 3-6 lists the resulting worst-case DMA temperature variations using this temperature coefficient and the temperature variations of the TRE boxes from Table 3-5.

Table 3-6. DMA temperature stability without active temperature control

Property	DMA Temperature Variation	
	A-Side	B-Side
Amplitude at Roll Frequency	1.15 mK	1.86 mK
Amplitude at Orbital Frequency	21.2 mK	21.2 mK
Amplitude at Annual Frequency	1.54 K	1.33 K
Linear Drift	0.74 K/yr	0.64 K/yr

3.8.2 PID Mode

In the PID mode the temperature is controlled using a PID controller with the STDS as the temperature sensor and the power dissipation in the DMA heater resistor as the control effort. In this mode, a worst-case peak-to-peak temperature variation of 26 mK has been demonstrated, which is limited by digitization and noise in the temperature readout system [Farley 2001a]. For the PID mode, the DMA temperature stability depends on the worst of either the 26 mK value above or the value found from the temperature coefficient of the SDTS temperature measurement.

The DMA temperature measurement sensitivity to the TRE box temperature depends on two factors: the temperature sensitivity of the 10 μA current bias for the SDTS and the temperature sensitivity of the STDS readout electronics, which measures the voltage across the STDS. At 72 K, the voltage across the SDTS is 1.036 V, the derivative of the SDTS temperature with respect to voltage across the SDTS is -602 K/V at 72 K [Farley 2003a], and the dynamic resistance of the SDTS is 849 Ω [Koç 1997].

A worst-case estimate of the sensitivity of the 10 μA SDTS current bias to TRE box temperature is based on an analysis of the TRE analog board schematic diagram [Lockheed 1998]. The two critical temperature dependent elements in this circuit are a 499 kΩ resistor, which has a worst-case temperature sensitivity of 5 ppm/K, and the Analog Devices REF02AZ voltage reference (part # 8551401PA), which has a worst-case temperature coefficient of 8.5 ppm/K [Analog Devices 2002]. Combining these values on a worst-case basis and using the temperature sensitivity and dynamic resistance of the silicon diode temperature sensor, we find a sensitivity of 69 μK [SDTS]/K [TRE].

A worst-case estimate of the sensitivity of the readout of the voltage across the STDS to the TRE box temperature is also based on an analysis of the TRE analog board schematic diagram [Lockheed 1998] and the schematic diagram of the SRE, which contains a buffer amplifier and an analog to digital converter. There are four sources for this sensitivity.

1. Input offset voltage. The input amplifier, which has a gain of 5, involves a pair of Analog Devices OP-97AZ/833s. The maximum average temperature coefficient of the input offset voltage for these OP-97s is 0.6 μV/K [TRE] [Analog Devices 2000a]. Taking twice this value and multiplying it by the derivative of the STDS temperature with respect to voltage across the SDTS, we find a sensitivity of 0.72 mK [SDTS]/K [TRE].
2. Input offset current. The temperature coefficient due to the temperature sensitivity of the input offset current is completely negligible because of the very small value of the offset current and the relatively low value of 849 Ω for the dynamic resistance of the STDS.
3. Voltage gain. The temperature sensitivity of the voltage gain of the amplifiers is governed by the temperature coefficients of 6 critical resistors, which have temperature coefficients no greater than 5 ppm/K. Using the voltage across the STDS and the derivative of the STDS temperature with respect to STDS voltage, we find a worst-case temperature coefficient of 18.7 mK [STDS]/K [TRE].
4. ADC. Using the temperature coefficient of 7 ppm/K for the Analog Devices AD780 voltage reference [Analog Devices 2000b], which is the reference for the 16 bit Analog Devices ADS7805 analog to digital converter, we find a temperature coefficient of 4.4 mK [STDS]/K [TRE].

Table 3-7. DMA temperature stability with temperature active control

Property	DMA Temperature Variation	
	A-Side	B-Side
Amplitude at roll frequency	13.0 mK (0.15 mK)	13.0 mK (0.25 mK)
Amplitude at orbital frequency	13.0 mK (2.9 mK)	13.0 mK (2.9 mK)
Amplitude at annual frequency	0.21 K	0.18 K
Linear drift	0.100 K/yr	0.086 K/yr

Combining on a worst-case basis the current bias and voltage readout sources of the temperature coefficient, we find a value of 23.9 mK [STDS]/K [TRE]. Table 3-7 lists the resulting worst-case DMA temperature variations either using this temperature coefficient and the temperature variations of the TRE boxes from Table 3-5 or the demonstrated 26 mK peak-to-peak value. In the cases where the 26 mK value dominates, the value based on the TRE temperature coefficient of the SDTS temperature is given in parentheses.

4 VERIFICATION OF BIAS AND SCALE-FACTOR REQUIREMENTS

The telescope subsystem is divided into two blocks: (1) the optical imaging subsystem, and (2) the telescope readout. The telescope readout includes the optical transport of the plus and minus beams split by the roof prism, the photodetectors that convert the photon fluxes to currents, and the analog and digital electronics. The interface between these blocks is at the roof prisms. Temperature variation is the major source that produces unmodeled errors associated with the requirements verified by this document. The only other significant source is aging due to stress relaxation and particle radiation. However, this latter source is only applicable to T003 requirements 7.6.2.4 "Linear Drift".

1. We assume that the science instrument is operating in its baseline science mode, without anomalies.
2. We assume a roll period of 3 minute or less during the science data taking period. The 3 minute roll period is compatible with the analysis of Kirschenbaum [Kirschenbaum 2002]. He found by analysis that the thrusters for the attitude and translational control system require a helium flow rate of 4.87 mg/s. The seasonal minimum available helium flow rate is 6.73 mg/s, which gives a margin of 38 %. Temperature variations for shorter roll periods are smaller due to passive filtering from the heat capacity and the thermal isolation of the critical items. Thus any scale-factor or angular-bias errors introduced by temperature variations at shorter roll periods are smaller.
3. We consider one axis of the telescope at a time. A transverse shift of the focal position, one of the roof edges, or the secondary mirror with respect to the axis of the telescope primary mirror is represented by the symbol Δx, which can be associated with either the x axis or y axis of the telescope.
4. The effects of telescope nonlinearity are not included in this verification document since they are covered by T002 requirement 7, which is verified by analysis in S0686 [Turneaure 2002b].
5. All unmodeled variations are considered as positive so that when they are added they represent a worst-on-worst case.
6. Verification of T003 requirements 7.6.2.1, 7.6.2.2, and 7.6.2.3 at roll frequency also represent verification of these requirements at the body-fixed SQUID calibration frequencies. The low frequency SQUID calibration frequency is either 1/124 Hz or 1/62 Hz [Whelan 2002]. Both of these frequencies are larger than the roll frequency associated with the 3 minute roll period. Temperature variations and thus variations in scale factor and bias at the low frequency SQUID calibration frequency are less than those at roll frequency both because of the added passive thermal filtering and the fact that the variations in thermal input are less at frequencies displaced from roll frequency. The high frequency SQUID calibration frequency is either 110 Hz or 220 Hz. Scale factor and bias variations due to temperature variations are negligible at these frequencies.
7. Unless otherwise specified, all equations are in SI units with angles in radians.

4.1 Optical Imaging Subsystem

We divide our analysis of the optical imaging subsystem into two parts: the probe windows and the telescope optics. The optical imaging subsystem introduces both scale-factor variations and bias variations. The measured telescope pointing angle θ_m is related to the normalized telescope signal S_n and to a scale factor b, which depends on the telescope focal length and optical aberrations in the telescope/window system (*i.e.* the image quality).

$$\theta_m = b\, S_n \tag{4-1}$$

During telescope verification at the payload level, Bernier *et al.* found the worst-case maximum value for b of 2.21×10^3 marcsec at a wavelength of 668 nm [Bernier 2002]. Using this value for 668 nm, an appropriate average b value of 2.29×10^3 marcsec across the 400 nm to 1000 nm band was found by Turneaure *et al.* [Turneaure 2002a]. Note that these references give values for the inverse of b.

The quantitative measure of defocus of the optical imaging system is given in waves at a wavelength of 700 nm, and it is represented by the symbol Δn. One wave of defocus corresponds to 1 wave of peak-to-valley phase difference across the diameter of the telescope primary mirror between a collimated wave and a spherical wave that brings the telescope back into focus. A defocus value of Δn can be converted to a fractional change in the factor b.

$$\frac{\Delta b}{b} = \frac{1}{b}\frac{db}{dn}\Delta n \tag{4-2}$$

The worst-case maximum value of $(db/dn)/b$ is 0.67 /wave based on telescope data taken during Payload verification and reported on page 12 of S0686 [Turneaure 2000b].

4.1.1 Probe Windows

The probe windows introduce both scale factor and bias variations. The dominating source for scale-factor variations is focal power variation driven by temperature variations of the windows. The dominating sources for bias variations are (1) temperature variations and, over long times, (2) particle radiation and stress relaxation.

4.1.1.1 Scale-Factor Variations

The probe windows influence the scale factor b defined in Eqn 4-1. A perfect, in-focus telescope produces the highest sensitivity for the normalized telescope pointing signal to angular displacement of the star, and thus the smallest value of b. The value of b is degraded (*i.e.* increases) by both defocus (for the small defocus values here, it is equivalent to a spherical aberration) and higher order optical aberration terms. As long as the thermal state of the windows is constant, the defocus and other aberrations remain constant, and thus the value of b also remains constant. A change in defocus produces a change in the factor b without any change in the bias angle assuming the windows are centered on the optical axis, which condition is appropriate for the window system.

During the course of the mission, any change in scale factor attributable to the windows arises from changes in the heat load on the window system from the space vehicle in the orbital environment. The thermal time constants of the windows range from a time of seconds to hours. The thermal response time in window #4, the outer window, is about 80 ms from one side to the other on a diameter line. The thermal response time is considerably longer for the fused-quartz windows. For a first order approximation, the temperature distribution across the windows is axially symmetric and is quadratic in the radius ρ. This type of temperature distribution leads to a defocus due to both the change in the figure of the window from thermal expansion and the change in the index of refraction with temperature. The following equation gives the defocus term in waves Δn_ρ at a wavelength of λ_0, where γ_W is the thickness of a window, α is the thermal expansion coefficient, η is the index of refraction, and ΔT_ρ is the temperature difference between the center of the window and the radius of the telescope clear aperture.

$$\Delta n_\rho = \frac{1}{\lambda_0} \Delta T_\rho \, \gamma_W \left[\alpha \, (\eta - 1) + \frac{d\eta}{dT} \right] \tag{4-3}$$

Wedel [Wedel 1998] investigated the temperature distribution of the windows and their time dependences. The defocus change is dominated by Window #4 and Window #3. Window #1 and Window #2 have much lower and smaller variations in heat loads and, being at lower temperature, lower expansion coefficients and temperature coefficients of the index of refraction. Although Window #4 has a larger heat load, its thermal conductivity is very much greater than that of fused quartz.

The radial temperature difference at orbital frequency is given in the following equation, where $\Delta T_{\rho,o,0}$ is the amplitude of the radial temperature difference at the orbital angular frequency ω_o.

$$\Delta T_{\rho,o} = \Delta T_{\rho,o,0} \sin(\omega_o \, t) \tag{4-4}$$

To find the daily drift in the radial temperature, we assume that the annual variation in the temperature is represented by the following equation, where the symbol $\Delta T_{\rho,a,0}$ is the annual temperature amplitude and ω_a is the annual angular frequency.

$$\Delta T_{\rho,a} = \Delta T_{\rho,a,0} \sin(\omega_a \, t) \tag{4-5}$$

We find the maximum daily drift rate by taking twice the maximum derivative of Eqn 4-5 with respect to time $[d(\Delta T_{\rho,a})/dt]_{\max}$. The reason for taking twice the value is to account for the possibility that the annual heat load variations may have higher harmonic contributions that lead to a greater maximum daily drift.

Finally, we calculate the percentage change in scale factor using Eqn 4-2. We make the worst-case estimates below at a wavelength of 700 nm, which represents a satisfactory average across the band.

Window #4. Table 4-1 is a list of the temperature distribution properties of Window #4 found in Figures 6, 7, 14 and 15 of EM No. TCS 217 [Wedel 1998] needed for this analysis. The symbol β is the angle between the axis of the space vehicle and the direction of the sun's rays. The sun is shining on the aft end of the space vehicle when β is equal to zero. The two values of β in the table correspond to the seasonal temperature extremes.

Table 4-1. Temperature distribution properties of Window #4

Angle between Space Vehicle Axis and the Sun, β	On-Axis Temperature	Radial Temperature Difference	Orbital Amplitude of Radial Temperature Difference
68°	237.6 K	-0.006 K	< 0.012 K
0°	209.7 K	+0.006 K	< 0.012 K

We now calculate the worst-case percentage amplitude in the scale factor at orbital frequency and the worst-case percentage drift of the scale factor for Window #4 using the properties listed in Table 3-2 and Table 4-1. We actually use twice the value of $d\eta/dT$ given in Table 3-2 for the reason given in section 3.1. The results are $\Delta b_{o,W4}/b$ = 0.26 % and $[d(\Delta b/b)/dt]_{max}$ = 0.01 %/day.

Window #3. Table 4-2 is a tabulation of the needed temperature distribution properties of Window #3 found in Figures 17, 18, 21 and 22 of EM No. TCS 217 [Wedel 1998]. The two values of β in the table correspond to the seasonal temperature extremes.

Table 4-2. Temperature distribution properties of Window #3

Angle between Space Vehicle Axis and the Sun, β	On-Axis Temperature	Radial Temperature Difference	Orbital Amplitude of Radial Temperature Difference
68°	112.7 K	0.92 K	0.015 K
0°	108.0 K	0.70 K	0.015 K

We now calculate the worst-case percentage amplitude in the scale factor at orbital frequency and the worst-case percentage drift of the scale factor for Window #3 using the properties listed in Table 3-3 and Table 4-2. The expansion coefficient and index of refraction, and its temperature coefficient in Table 3-3 are room temperature values. They can be considered worst-case values since Window #3 is at temperatures below room temperature. The results are $\Delta b_{o,W3}/b$ = 0.23 % and $[d(\Delta b/b)/dt]_{max}$ = 0.06 %/day.

Summary. Table 4-3 lists the sum of the worst-on-worst contributions to the scale-factor variations for Window #4 and Window #3.

Table 4-3. Contribution of windows to scale-factor variations

Requirement	Title	Worst-Case Value
T003: 7.6.3.1	Orbital Frequency Scale Factor Variation	0.49 % (amplitude)
T003: 7.6.3.2	Linear Drift in Telescope Scale Factor	0.07 %/day

4.1.1.2 Bias Variations

The window subsystem introduces angular bias variations in the guide star wavefront reaching the telescope due to linear transverse temperature variations across the windows. This bias variation is completely dominated by Window #4 and Window #3 since the colder windows (Window #1 and Window #2), which are very well isolated from exterior of the space vehicle, see substantially smaller transverse thermal loads. The linear transverse temperature variation across a window yields an angular bias variation $\Delta\theta_{b,W}$ according to the following equation where ΔT_d is the temperature difference across a diameter d_W of a window, α is the thermal coefficient of expansion, η is the index of refraction, and $d\eta/dT$ is the temperature coefficient of the index of refraction, and γ_W is the window thickness.

$$\Delta\theta_{b,W} \cong \frac{1}{d_W}\left\{\Delta T_d\ \gamma_W\left[\alpha\,(\eta-1)+\frac{d\eta}{dT}\right]\right\} \tag{4-6}$$

Using the properties for Window #4 in Table 3-2 with the value of $d\eta/dT$ set to twice the value in the table for the reason given in section 3.1 and for Window #3 in Table 3-3, Eqn 4-6 reduces to the following forms.

$$\Delta\theta_{b,W4} = 2.24\times10^{-7}\,\frac{\Delta T_d}{d_W}\ \text{for Window \#4} \tag{4-7}$$

$$\Delta\theta_{b,W3} = 1.63\times10^{-7}\,\frac{\Delta T_d}{d_W}\ \text{for Window \#3} \tag{4-8}$$

The values of ΔT_d and related d_W are discussed in the sections below.

4.1.1.2.1 Roll-Frequency Bias Variations

The only significant source of roll-frequency bias variation for the windows is variation in the transverse temperature gradient at roll frequency for each of the windows. This source is completely dominated by the contributions from Window #4 and Window #3 since Window #1 and Window #2 are very well isolated from transverse temperature gradients at roll frequency.

Window #4. The transverse temperature gradient of Window #4 at roll frequency was analyzed by Wedel [Wedel 1998]. The mounting flange for Window #4 has an edge-to-edge temperature difference amplitude of 0.13 K for a 3 minute roll period. The temperature difference across Window #4 is greatly reduced because of the low thermal conduction between the window and its frame compared to the high thermal conduction across the window. Inspection of Fig. 12 and Fig. 13 found in EM No. TCS 217 [Wedel 1998] indicates that the edge-to-edge temperature difference amplitude across Window #4 for a 3 minute roll period does not exceed 20 μK. Instead of using the diameter of Window #4 as the edge-to-edge distance, we use a more conservative value of 5.66 inch, which is the outside diameter of the telescope clear aperture. Using these values, Eqn 4-7 yields a bias angle amplitude of 3.12×10^{-11} rad (0.00643 marcsec) for a 3 minute roll period.

Window #3. The transverse temperature gradient at roll frequency of Window #3 was also analyzed by Wedel [Wedel 1998]. Inspection of Fig. 23 found in EM No. TCS 217 [Wedel 1998] indicates that the temperature difference amplitude across Window #3 for a 3 minute roll period does not exceed 10 μK. Using this value and the conservative 5.66 inch diameter, Eqn 4-8 yields a bias angle amplitude of 1.13×10^{-11} rad (0.00234 marcsec) for a 3 minute roll period.

Summary. Table 4-4 lists the worst-case values due to the window system for each of the three roll-frequency bias variation requirements. The linear variation is found by summing the contributions from Window #4 and Window #3 and by assuming that this value can linearly drift from a negative value to a positive value over one year. The annual and orbital variations are found by summing the contributions from Window #4 and Window #3.

Table 4-4. Window contributions to roll-frequency bias variations

Requirement	Title	Worst-Case Value
T003: 7.6.2.1	Linear Variation	0.0176 marcsec/yr
T003: 7.6.2.2	Annual Variation	0.0088 marcsec
T003: 7.6.2.3	Orbital Variation	0.0088 marcsec

4.1.1.2.2 Body-Fixed Bias Variations

The body-fixed bias variations introduced by the window system can be the result of transverse temperature gradient variations in the windows and long-term effects due to stress relaxation and particle radiation.

First we give an estimate of possible long-term effects due to stress relaxation and particle radiation damage. For high grade optical materials, such long-term effects should correspond to changes of less than 0.01 waves otherwise the windows could degrade a telescope image over time (*e.g.*, the Hubble Space Telescope has maintained its optical figure over many years in earth orbit). For optical materials, stress relaxation is known to not degrade optical components of even much larger size over very long periods of time. Damage due to particle radiation should be small for the particle fluence seen by the windows over a one year period and further the effect to first order will be uniform over a window and roll averaging reduces even further the possibility of changes in the transverse gradient of the optical path length. If in any case we assume a linear change of 0.01 wave across the telescope clear aperture (5.66 inch), and use the mid-band wavelength of 700 nm, we calculate that this change yields an angular bias of 4.87×10^{-8} rad (10.0 marcsec). Since the particle radiation is to first order uniform over time and the windows have had a long time to relax, this angular bias should appear as a linear drift in time and in the worst-case amount to 4.87×10^{-8} rad/yr (10.0 marcsec/yr) per window, giving a worst-on-worst total of 1.95×10^{-7} rad/yr (40.0 marcsec/yr).

Window #4. The transverse temperature gradient for Window #4 was analyzed by Wedel [Wedel 1998]. From Fig. 4 and Fig. 5 found in EM No. TCS 217 [Wedel 1998], the maximum edge-to-edge temperature difference is 9.3 mK. Again we conservatively assume that the distance associated with this temperature difference is the diameter of the telescope clear aperture, which is 5.66 inch. Using Eqn 4-7, we find a body-fixed angular bias of 1.45×10^{-8} rad (2.99 marcsec). Assuming a worst-case condition, the body-fixed amplitude at any frequency can not exceed 1.45×10^{-8} rad (2.99 marcsec), and the worst-case linear drift over one year is at most twice this value 2.90×10^{-8} rad/yr (5.98 marcsec/yr).

<u>Window #3</u>. The transverse temperature gradient for Window #3 was analyzed by Wedel [Wedel 1998]. From Fig. 23 found in EM No. TCS 217 [Wedel 1998], the maximum edge-to-edge temperature difference is 8.2 mK. Again we conservatively assume that the distance associated with this temperature difference is 5.66 inch. Using Eqn 4-8, we find a body-fixed angular bias of 9.30×10^{-9} rad (1.92 marcsec). Assuming a worst-case condition, the body-fixed amplitude at any frequency can not exceed 9.30×10^{-9} rad (1.92 marcsec), and the worst-case linear drift over one year is 1.86×10^{-8} rad/yr (3.84 marcsec/yr).

<u>Summary</u>. Table 4-5 lists the worst-on-worst values due to the window system for each of the two body-fixed bias variation requirements. The linear drift is found by summing the contribution from stress relaxation and particle radiation and the temperature gradient contributions from Window #4 and Window #3, and further by assuming that it takes place over one year. The variations at other frequencies are found by summing the temperature gradient contributions from Window #4 and Window #3.

Table 4-5. Window contributions to body-fixed bias variations

Requirement	Title	Worst-Case Value
T003: 7.6.2.4	Linear Drift	50 marcsec/yr
T003: 7.6.2.5	Bias Variations at Other Frequencies	4.9 marcsec

4.1.2 Telescope Optics

The telescope, located in the vacuum probe at low temperature, is at a temperature of less than 5 K. There are two heat sources: (1) the thermal radiation coming down the probe which is primarily deposited at the forward end of the telescope, and (2) an electrical power of 3.2 mW dissipated in the DMAs needed both to heat the JFET preamplifiers to about 72 K on thermal standoffs for proper operation and for powering the preamplifiers. The thermal radiation is specified to be less than 0.25 mW. However, an analysis [Burns 2002] demonstrates a much smaller value that is less than 0.010 mW. Although the heat power variations and resulting temperature variations are small, the nature of the telescope design increases the sensitivity to these temperature variations. Long-term bias effects due to stress relaxation and particle radiation are very small and can be neglected since the telescope is much better shielded from particle radiation than the windows, particularly Window #4.

Appendix 1 is a *Mathematica®* notebook that traces optical rays through the telescope to find the axial and transverse focal position. Table 4-6 is a list of some of the telescope properties found with this notebook. The symbol ΔL represents a small change in the length of the metering tube about its nominal value, and the symbol R_{SM} is the spherical radius of the secondary mirror, which is convex. This *Mathematica*® notebook also calculates the pointing angle bias shift due to bending of the metering tube, which results in a transverse position shift of the secondary mirror and the roof prisms and an angular tilt of the secondary mirror.

Table 4-6. Telescope properties found with the ray trace notebook

Property	Value
Focal length	3.566 m
Derivative of the number of waves of defocus with respect to ΔL	16.1 waves/mm
Derivative of waves of defocus with respect to % change in R_{SM}	7.40 waves/%

Appendix 2 is a *Mathematica*® notebook that calculates the response of the telescope to thermal power input at its forward plate. It assumes a worst-case condition in which the forward end of the metering tube and the secondary mirror are at 6 K and the aft end of the metering tube, the primary mirror and secondary mirror are at 2.5 K. The heat power derived by the *Mathematica*® notebook is 3.5 mW, which is conservative since the total power dissipated by the DMAs is 3.2 mW [see section 3.8]. Temperature measurements of the telescope forward plate during payload verification on 6 Aug 2001 give a temperature of 3.73 K for a heat power of 6.0 mW [Farley 2001b], which shows that the 6 K value is very conservative. This lower measured temperature may be in part the result of some of the power dissipation being shunted directly to the probe through the electrical conductors between the probe and the DMAs. The analysis in Appendix 2 assumes a thermal expansion coefficient derived from the thermal expansion data [Touloukian 1977] for pure fused quartz with a fictive temperature of 1273 K. The analysis assumes the recommended temperature coefficient of thermal conduction for high-purity clear fused quartz [Touloukian 1970a].

The heat power input into the telescope forward plate at roll and orbital frequencies is dominated by the heat power variation coming from the four DMAs rather than from the thermal radiation. Appendix 3 is a *Mathematica*® notebook that calculates the amplitude of the thermal radiation power at roll and orbital frequencies coming down the probe neck to the SIA using a simple worst-case model. This calculation uses data for the specific heat of fused quartz [Touloukian 1970b], the window temperatures and heat powers entering the top side of the windows (found in EM No. TCS 342B) [Burns 2002]. The analysis in the notebook gives amplitudes of 0.10 pW at roll frequency and of 7.2 nW at orbital frequency. The actual amount at roll frequency could be somewhat larger due to thermal radiation sneak paths, but in any case it is very much less than the worst-case heat power amplitude due to the power dissipation amplitude at roll frequency in the four

DMAs. The worst-case heat power amplitudes applied to the telescope forward plate, due to temperature variations of the DMAs, are found from the worst-case DMA temperature variations from Table 3-6 and Table 3-7, which are 13 mK at roll frequency and 21.2 mK at orbital frequency. Using the total thermal conduction coefficient of 47.8 μW/K for all four DMAs from section 3.8.1 yields a worst-case heat power amplitude of 0.62 μW at roll frequency and 1.01 μW at orbital frequency.

The heat power variations at annual frequency of the telescope and the linear temperature drift of the telescope are again dominated by heat power variations coming from the four DMAs rather than from the thermal radiation coming down the probe neck. An analysis by Burns [Burns 2002] gives a value for the thermal radiation of less than 10 μW. This changes very little over the year and certainly less than 5 μW. Using the 5 μW value leads to a heat power amplitude at annual frequency of 2.5 μW and a very worst-case drift in the heat power of 5.0 μW/yr. We find the worst-case heat power variation coming from the DMAs using the worst-case temperature annual amplitude and drift values from Table 3-6 and Table 3-7, which are an amplitude of 1.54 K at annual frequency and a drift 0.74 K/yr. Using the total thermal conductivity of 47.8 μW/K for the four DMAs gives a heat power amplitude at annual frequency of 73.6 μW and a heat power drift rate of 35.4 μW/yr. Summing the two sources of heat power variation gives a heat power amplitude at annual frequency of 76.1 μW and a heat power drift rate of 40.4 μW/yr.

Table 4-7 lists the worst-case heat power variations at the telescope forward plate.

Table 4-7. Worst-case heat power variations at telescope forward plate

Property	Value
Heat power amplitude at roll frequency	0.62 μW
Heat power amplitude at orbital frequency	1.01 μW
Heat power amplitude at annual frequency	76.1 μW
Drift rate of heat power	40.4 μW/yr

4.1.2.1 Scale-Factor Variations

The telescope optics can introduce scale-factor variations due to variations in its temperature distribution that change the focal position and thus the value of the scale factor *b* in Eqn 4-1, which converts the normalized telescope pointing signal to a pointing angle. There are three sources that change the focal length of the telescope: (1) a length change in the telescope metering tube, (2) a radius change in the telescope secondary mirror, and (3) a focal power change in the telescope forward plate.

The telescope is made from Herasil[†] fused quartz, which is very homogeneous and for which the temperature coefficient of expansion is very uniform throughout the material.

[†] Product of Heraeus Amersil.

Thus the telescope remains geometrically similar when it is cooled from room temperature to low temperature, and the focal position remains nearly fixed with respect to the roof prisms. However, under the low-temperature operating conditions the temperature distribution is not completely uniform because of the heat power entering the telescope forward plate. The primary mirror and the tertiary mirror are both bonded to the telescope baseplate at the aft end of the metering tube, and thus they are at essentially the same temperature. There is a temperature gradient along the metering tube due to heat flow from the forward end to the aft end. The telescope forward plate is attached at the forward end of the metering tube. The secondary mirror is bonded to the forward plate. Thus the forward end of the metering tube and the secondary mirror are nearly at the same temperature.

Metering Tube and Secondary Mirror. The *Mathematica*® notebook listed in Appendix 2 calculates the derivative of the fractional scale-factor with respect to added heat power at the telescope forward plate $(db/dP)/b$, where P is the heat power entering the telescope forward plate. The result is -5.31 %/W.

We find the worst-case orbital variation in the scale factor using the worst-case heat power amplitude at orbital frequency of 1.01 μW from Table 4-7. Using this value and the 5.31 %/W factor yields a maximum fractional scale-factor amplitude of $\Delta b_{o,MT}/b$ = 5.36×10^{-6} % at orbital frequency, which is clearly negligible.

We find the worst-case linear drift over a one day period using the annual variation in the heat power P_a into the telescope forward plate from Table 4-7.

$$P_a = 76.1\times10^{-6} \sin(\omega_a\, t) \tag{4-9}$$

The worst-case drift rate over one day is found by taking twice the maximum derivative with respect to time of Eqn 4-9, which is 2.62 μW/day. We use twice the maximum derivative to account for possible higher harmonic content in the annual variation. Using this value and the 5.31 %/W factor yields a maximum daily drift rate of $[d(\Delta b/b)/dt]_{\max}$ = 1.39×10^{-5} %/day, which again is clearly negligible.

Forward Plate. The same considerations that were applied to Window #3 and Window #4 apply to the determination of the focal power introduced by the telescope forward plate. In particular, we use Eqn 4-3 with the appropriate forward plate parameters applied. We find an equation for the worst-case value of the temperature difference ΔT_p between the center of the forward plate and its outside diameter using the following assumptions.

1. The heat power P is assumed to be applied uniformly over the surface of the forward plate. This is a worst-case assumption since almost all of the heat power entering the telescope forward plate comes from the DPAs, which are located near the outside diameter of the forward plate.
2. The heat power is conducted to the outside diameter of the forward plate and then down the metering tube

3. The heat power flow is assumed to be uniform over the thickness γ_{FP} of the forward plate. This assumption is satisfactory since the thickness to radius ratio for the forward plate is 0.11.
4. The thermal conductivity κ is assumed to be a constant, which is satisfactory because of the small temperature changes within the forward plate.

$$\Delta T_\rho = \frac{P}{4\,\pi\,\kappa\,\gamma_{FP}} \tag{4-10}$$

Substituting ΔT_ρ into Eqn 4-3 modified for the forward plate yields the following equation for Δn_ρ.

$$\Delta n_\rho = \frac{P}{4\,\pi\,\lambda_0\,\kappa}\left[\alpha\,(\eta-1)+\left(\frac{d\eta}{dT}\right)\right] \tag{4-11}$$

From Table 4-7, the maximum heat power at orbital frequency entering the forward plate has an amplitude of 1.01 μW. Using the room temperature values for the index of refraction and its temperature coefficient from Table 3-3, the wavelength at the center of the band 700 nm, and the values of α = -6.33×10^{-8} /K [Touloukian 1977] and κ = 1.03×10^{-1} W/m/K [Touloukian 1970a] both at 6 K give a value of Δn_ρ of 1.08×10^{-5} waves. Multiplying this value by the factor 0.67 /wave gives a scale-factor amplitude at orbital frequency of $\Delta b_{o,FP}/b$ = 0.0007 %.

Using the same approach as for the metering tube, the maximum heat power drift rate over a day is 2.62 μW/day. Using the same values as in the previous paragraph for the index of refraction and its temperature coefficient, the wavelength at the band center, α, and κ gives a value of Δn_ρ of 2.81×10^{-5} waves/day. Multiplying this value by the factor 0.67 /wave gives a scale-factor drift rate over 1 day of $[d(\Delta b/b)/dt]_{max}$ = 0.0019 %/day.

Summary. Table 4-8 lists the worst-on-worst contributions for the telescope metering tube, secondary mirror, and forward plate due to heat power input variations at the forward plate, which is dominated by the contribution from the forward plate.

Table 4-8. Contribution of telescope optics to scale-factor variations

Requirement	Title	Worst-Case Value
T003-7.6.3.1	Orbital Frequency Scale Factor Variation	0.0007 % (amplitude)
T003-7.6.3.2	Linear Drift in Telescope Scale Factor	0.0019 %/day

4.1.2.2 Bias Variations

The dominating source for angular bias variations introduced by the telescope is temperature variation due to the variation in heat dissipation in the telescope structure. There are two sources for angular bias variations within the telescope: (1) transverse heat flow in the metering tube resulting in its bending and (2) transverse heat flow in the forward plate resulting in an optical wedge.

Metering Tube. There are three effects due to transverse heat flow in the metering tube and thus its bending: (1) a transverse position shift of the roof edge position, (2) a transverse position shift of the center of the secondary mirror, and (3) an angular tilt of the secondary mirror. The two position shifts, which are identical, and the tilt are with respect to the common axis for the primary and tertiary mirrors. Here we make a worst-case calculation of the tilt $\Delta\phi_S$ of the forward plate due to a transverse heat flow in the metering tube using the following assumptions.

1. The metering tube is an annular cylinder with a length L, an outside diameter d_o and an inside diameter d_i. The ratio of the thickness of the annulus $(d_o - d_i)/2$ to ½ of the average circumference $\pi (d_o + d_i) / 4$ is 0.03. This small ratio allows us to assume in our thermal calculation that the wall thickness is thin compared to the length over which the heat power is transported.
2. We assume a transverse heat power flow $P_{T,MT}$ in the metering tube that is uniformly distributed along the length and the wall thickness of the metering tube.
3. We assume that the nominal temperature of the metering tube is at the temperature of the forward end of the telescope T_{FP} since that temperature gives a worst-case value of the ratio of the thermal expansion coefficient α to the thermal conductivity κ.
4. A worst-case estimate of the tilt angle $\Delta\phi_S$ is assumed to be the differential expansion across the metering tube diameter over the length of the metering tube divided by the diameter of the metering tube. Elastic effects are assumed to be small.

The resulting equation for $\Delta\phi_S$ is as follows.

$$\Delta\phi_S = \frac{\alpha(T_{FP})}{\kappa(T_{FP})} \frac{\pi}{2} \frac{1}{d_o - d_i} P_{T,MT} \tag{4-12}$$

Using the values for d_o and d_i from Table 3-4, the thermal expansion α [Touloukian 1977] and thermal conductivity coefficient κ [Touloukian 1970a] both for fused-quartz at 6 K yields the following numerical form.

$$\Delta\phi_S = 6.33 \times 10^{-5} \; P_{T,MT} \tag{4-13}$$

We now estimate the transverse position shift of the forward plate and thus the transverse position shift in the secondary mirror and a roof edge. We assume that the axis of the metering tube undergoes an angle change from the baseplate to the forward plate that is linear in position along the metering tube length, which is clearly a worst-case assumption since the transverse heat power flow tends to be larger at the forward end of the metering tube. This assumption results in a forward plate position shift Δx_{FP} of the following form.

$$\Delta x_{FP} = \frac{L}{2} \Delta\phi_S \tag{4-14}$$

Using the length of the metering tube from Table 3-4, we find the following form.

$$\Delta x_{FP} = 1.10 \times 10^{-5}\ P_{T,MT} \tag{4-15}$$

The transverse position shift Δx_F of the focal position (relative to the axis of the primary mirror) due to the transverse position shift and the tilt of the secondary mirror is found using the *Mathematica*® notebook listed in Appendix 1. The result is represented by the following equation.

$$\Delta x_F = -2.34 \times 10^{-4}\ P_{T,MT} \tag{4-16}$$

The angular bias shift $\Delta\theta_{b,MT}$ due to bending of the metering is expressed by the following equation, where f is the focal length of the telescope.

$$\Delta\theta_{b,MT} = \frac{\Delta x_f - \Delta x_{FP}}{f} = 6.87 \times 10^{-5}\ P_{T,MT} \tag{4-17}$$

Forward Plate. Transverse heat flow in the telescope forward plate and the resulting transverse temperature variation produces a wedge in the forward plate thickness as well as a wedge in its dielectric constant. Equation 4-6 with the appropriate parameters also applies to this case where $\Delta\theta_{b,FP}$ is the forward plate contribution to the angular bias in the measured angle, R_{FP} is the radius of the forward plate, ΔT_d is the temperature change across the diameter of the forward plate.

$$\Delta\theta_{b,FP} \cong \frac{1}{2\,R_{FP}} \left\{ \Delta T_d\ \gamma_{FP} \left[\alpha\,(\eta - 1) + \frac{d\eta}{dT} \right] \right\} \tag{4-18}$$

We now make a simple worst-case calculation of the temperature difference across the forward plate using the following assumptions, which yield a constant transverse temperature gradient across the forward plate.

1. The transverse heat power flow $P_{T,FP}$ into the outside diameter of the plate has the form: $(P_{T,FP}/2)\cos(\varphi)$. The symbol φ is the angle around the forward plate axis.
2. The thermal conductivity κ is adequately represented by a constant throughout the forward plate.
3. The forward plate is a round plate with radius R_{FP} and thickness γ_{FP}.

With these assumptions, the value of ΔT_d across the diameter of the forward plate is represented by the following equation.

$$\Delta T_d = \frac{P_{T,FP}}{\kappa\,\gamma_{FP}} \tag{4-19}$$

Thus, the angular bias change for the wavefront passing through the forward plate is represented by the following equation.

$$\Delta\theta_{b,FP} \cong \frac{P_{T,FP}}{2\,R_{FP}\,\kappa} \left[\alpha\,(\eta - 1) + \frac{d\eta}{dT} \right] \tag{4-20}$$

We now make a worst-case estimate of all quantities except for $P_{T,FP}$ in Eqn 4-20 using the knowledge that the forward-plate temperature is less than 6 K. At 6 K, the value of α

is -6.33 × 10^{-8} [Touloukian 1977] and the value of κ is 0.103 W/m/K [Touloukian 1970a]. We use the room temperature values for η and $d\eta/dT$, which are worst-case values. From Table 3-3 they are η = 1.455 and $d\eta/dT$ = 9.7 × 10^{-6}. Further for a worst-case estimate, we use the absolute values of the two terms, which when using the radius of the telescope clear aperture and thickness of the forward plate results in the following equation.

$$\Delta\theta_{b,FP} = 5.13\times10^{-4}\ P_{T,FP} \tag{4-21}$$

The numerical value in this equation is dominated by the second term in Eqn 4-20, which is itself probably too large because of the use of the room temperature value of $d\eta/dT$.

Telescope. The total angular bias error $\Delta\theta_{b,T}$ introduced in the telescope is the sum of Eqn 4-17 and Eqn 4-21.

$$\Delta\theta_{b,T} = \Delta\theta_{b,MT} + \Delta\theta_{b,FP} = (6.87\times10^{-5}\ P_{T,MT} + 5.13\times10^{-4}\ P_{T,FP}) \tag{4-22}$$

The appropriate values of of the transverse heat flows at roll frequency and long-term changes in the body-fixed frame are discussed in the sections below.

4.1.2.2.1 Roll-Frequency Bias Variations

From Table 4-7 the worst-case heat power amplitude at roll frequency into the telescope forward plate is an amplitude of 0.62 μW. Of this total heat power at most ½ of it flows in the transverse direction. Further we assume that this transverse heat flow is equally distributed between the forward plate and metering tube, *i.e.* $P_{T,FP} = P_{T,MT}$ = 0.155 μW. Using this value in Eqn 4-22 gives an angular bias roll component of 9.02 × 10^{-11} rad or 0.019 marcsec. Assuming the worst possible variation in the phase or amplitude of this roll component yields a linear drift of 0.038 marcsec/yr and an amplitude at orbital and annual frequencies of 0.019 marcsec. The telescope optics contributions to the roll-frequency bias variations are listed in Table 4-9.

Table 4-9. Telescope optics contributions to roll-frequency bias variations

Requirement	Title	Worst-Case Value
T003: 7.6.2.1	Linear Variation	0.038 marcsec/yr
T003: 7.6.2.2	Annual Variation	0.019 marcsec
T003: 7.6.2.3	Orbital Variation	0.019 marcsec

4.1.2.2.2 Body-Fixed Bias Variations

From Table 4-7 the worst-case power variations are a linear drift of 40.4 μW/yr and an amplitude to 76.1 μW at annual frequency. The amplitude at orbital frequency is substantially smaller at 1.01 μW. Again we assume that only ¼ of each of these values appears as a transverse heat flow variation in the forward plate and also in the metering tube. Using Eqn 4-22 and 10.1 μW/yr gives a linear drift in the angular bias of 5.88 × 10^{-9} rad/yr or 1.21 marcsec/yr. Using Eqn 4-22 and the transverse heat power amplitude of 19.0 μW at annual frequency gives a worst-case amplitude at other frequencies of 1.11×10^{-8} rad or 2.28 marcsec. The angular bias variation at annual frequency is the worst-case for frequencies at or above annual frequency. The telescope optics contributions to the body-fixed bias variations are listed in Table 4-10.

Table 4-10. Telescope optics contributions to body-fixed bias variations

Requirement	Title	Worst-Case Value
T003: 7.6.2.4	Linear Drift	1.21 marcsec/yr
T003: 7.6.2.5	Bias Variations at Other Frequencies	2.28 marcsec

4.2 Telescope Readout

The telescope readout system has four sections: (1) the transport of the plus and minus beams from the roof prism to the photodetectors using mirrors and lenses, (2) the photodetectors, (3) the analog electronics, which includes JFET preamplifiers located in the two Detector Package Assemblies (DPAs) mounted on the forward plate of the telescope, and the Telescope Readout Electronics box (TRE) that contains the remainder of the telescope analog electronics located within the Forward Equipment Enclosure (FEE), and (4) the telescope digital electronics located in the SQUID Readout Electronics box (SRE), which is also within the FEE.

After resetting the charge integrating feedback capacitors, the telescope readout electronics integrates the photocurrents for the plus and minus channels for just under 0.1 s. The integrating capacitor is again reset and the photocurrent integrations are begun again. This process is undertaken at a 10 Hz rate. The voltage ramp at the output of each charge locked loop is conditioned to an appropriate voltage range and then digitally recorded at a 2200 Hz rate using a high quality 16-bit analog to digital converter (ADC) with a temperature controlled reference voltage. The plus and minus photocurrents are derived from the slope $dV^{+/-}/dt$ of the recorded voltages. These derivatives are a measure of the plus and minus photocurrents, which are in turn a measure of the plus and minus photon fluxes at the entrance to the roof prism. A normalized telescope pointing signal is found by multiplying the slopes by appropriate efficiency factors, which include the effects of the optical transport efficiency from the image division at the roof prism to the photodetectors, the quantum efficiency of the photodetectors, the current-to-voltage conversion factors of the charge locked loops that produce the voltage ramps, and the voltage gains that condition the signals in front of the ADC. The normalized telescope pointing signal S_n is a function of the plus and minus photocurrents $i^{+/-}$ derived from the voltage ramps and the relative efficiency (or gain) factors $a^{+/-}$ due to the relative efficiencies in the two paths from the roof prism. The relative fractional difference variation of the $a^{+/-}$ is δ.

$$S_n = \frac{a^+ (1+\delta) i^+ - a^- (1-\delta) i^-}{a^+ (1+\delta) i^+ + a^- (1-\delta) i^-} \tag{4-23}$$

It is clear from Eqn 4-23 that the normalized telescope signal does not depend on both a^+ and a^-, but only on the ratio a^+/a^-. Thus S_n does not depend on the absolute intensity of the guide star or the absolute scale factor of the electronics. The measured telescope pointing angle θ_m is found by multiplying the normalized telescope signal by the scale factor b defined in Eqn 4-1.

To first order in the true pointing angle θ, the plus and minus photon fluxes $\xi^{+/-}$ incident on the roof prism are given by the following equation, where ξ_0 is the flux for both the plus and minus sides when the telescope is null pointed, and σ is scale factor for the term linear in θ.

$$\xi^{+/-} = \xi_0 \pm \sigma\,\theta \tag{4-24}$$

The relative efficiencies $a^{+/-}$ can be defined in such a way that the following relationship between $i^{+/-}$ and $\xi^{+/-}$ is appropriate.

$$\xi^{+/-} = a^{+/-}\; i^{+/-} \tag{4-25}$$

By combining these equations, we find the measured pointing angle θ_m to first order in δ and θ.

$$\theta_m = b\left(\delta + \frac{\sigma}{\xi_0}\,\theta\right) \tag{4-26}$$

We find the angular bias $\Delta\theta_{b,R}$ due to the relative mismatch between a^+ and a^- by setting the true pointing angle to zero.

$$\Delta\theta_{b,R} = b\,\delta \tag{4-27}$$

There is no error term in the scale factor because of the assumption that $\xi^{+/-}$ depend only linearly on θ. The worst-case maximum value of b, which is 2.29×10^3 marcsec [Turneaure 2002a], is used in the worst-case estimates below. Also the scale factor does not depend on the absolute values of the efficiencies because of the nature of the normalization. The effects of nonlinearity in $\xi^{+/-}$ introduced by the telescope optics is covered in T002 requirement 7, which is verified by the analysis in S0686 [Turneaure 2002b].

The unmodeled error for each electronic section is found by the worst-case uncertainty of variation of δ for that section. There is an initial uncertainty in δ due to calibration accuracy. The initial uncertainty of 2δ, estimated in S0686 [Turneaure 2002b], was found to be 0.78 % on a worst-case basis (99 % probability). This small uncertainty validates our consideration of using only the first order term in δ. Here we are only concerned with variations from this initial uncertainty. Note than an unmodeled error of 0.1 marcsec corresponds to a variation in δ of 0.0044 %.

4.2.1 Temperature Dependence of the Angular Bias

We find the temperature dependence of the differential gain for each section of the telescope readout chain below.

4.2.1.1 Transport of Plus/Minus Beams to the Photodetectors

The transport optics for the plus and minus sides of the divided image contributes a negligible amount to the bias variation. First the reflectivity/transmission of the mirrors and beam splitters are very stable since the films are overcoated with SiO and they are in a low-temperature (< 5 K), ultrahigh vacuum environment. Second changes in the image position and focus at the photodetectors due to temperature changes of the telescope forward plate are very small with the result that there is no significant change in the photocurrent outputs for the pair of detectors. Even these insignificant changes in efficiency are further reduced as long as the changes are the same for both the plus and minus beams because of the normalization. The result is that there is no credible contribution to unmodeled bias variations from this section.

4.2.1.2 Photodetectors Quantum Efficiency

The only source of the fractional differential efficiency variation δ_{QE} due to variation of the photodetector quantum efficiency is the temperature variation of the photodetectors. The fractional differential efficiency variation depends on the temperature coefficient of the fractional quantum efficiency k_{QE}, the temperature variation of the DMA ΔT_{DMA} on which the photodetectors are mounted, and a differential matching factor r_{QE}.

$$2\,\delta_{QE} = k_{QE}\; r_{QE}\; \Delta T_{DMA} \tag{4-28}$$

We find the temperature coefficient k_{QE} from the following equation for the conversion efficiency Q_c of photons to electron-hole pairs, where $R(\lambda)$ is the reflection coefficient at the surface of the photodetector, $\chi(\lambda,T)$ is the photon absorption coefficient in the photodetector, and γ_{PD} is the appropriate thickness of the photodetector.

$$Q_c = [1 - R(\lambda)]\,\{1 - \exp[-\chi(\lambda,T)\,\gamma_{PD}]\} \tag{4-29}$$

Rajkanan *et al.* [Rajkanan 1979] produced the following empirical form for the absorption coefficient $\chi(\lambda,T)$ in Si based on the theory of Hall *et al.* [Hall 1954] good to 20 % over the wavelength range of 310 nm to 1127 nm and the temperature range from 20 K to 500 K, where h is Planck's constant, k is Boltzmann's constant, c is the velocity of light, λ is the photon wavelength, and T is the temperature. The other symbols in this equation and their values are defined in Table 4-11.

$$\chi(\lambda,T) = \sum_{\substack{i=1,2\\ j=1,2}} C_i\, A_j \left[\frac{\{(h\,c/\lambda) - E_{gj}(T) + E_{pi}\}^2}{\exp\{E_{pi}/(k\,T)\} - 1} + \frac{\{(h\,c/\lambda) - E_{gj}(T) - E_{pi}\}^2}{\exp\{E_{pi}/(k\,T)\} - 1} \right] + A_c\,\{h\,c/\lambda - E_{gd}\}^{1/2} \tag{4-30a}$$

$$E_{gi}(T) = E_{gi}(0) - \frac{g_1\,T^2}{T + g_2} \tag{4-30b}$$

The first terms under the summation sign require phonon assisted transitions and the second term involves a direct transition. Any term for which the net energy in the curly brackets is less than or equal to zero has a value of zero. For a wavelength of 400 nm and greater, the net energy for the direct transition is less than zero (*i.e.* $h\,c/\lambda < E_{gd}$), and thus in our wavelength band it gives no contribution to the absorption coefficient.

Table 4-11. Parameter values for empirical form of photo absorption coefficient in Si

Description	Symbol	Value
Indirect gap 1 .	$E_{g1}(0)$	1.1557 eV
Indirect gap 2	$E_{g2}(0)$	2.5 eV
Direct gap	E_{gd}	3.2 eV
Acoustic DeBye temperature	E_{p1}	1.287×10^{-2} eV
Optical DeBye temperature	E_{p2}	5.773×10^{-2} eV
Constant associated with E_{p1}	C_1	5.5
Constant associated with E_{p1}	C_2	4.0
Constant associated with E_{p2}	A_1	3.231×10^{2} cm^{-1} eV^{-2}
Constant associated with E_{g1}	A_2	7.237×10^{3} cm^{-1} eV^{-2}
Constant associated with E_{g2}	A_d	1.052×10^{6} cm^{-1} eV$^{-1/2}$
Constant	g_1	7.021 10^{-4} eV/K
Constant	g_2	1108 K

Appendix 4 is a listing of a *Mathematica*® notebook that calculates the average value of $(dQ_c/dT)/Q_c$ across the 400 nm to 1000 nm band assuming that the number of photons per second per unit wavelength is constant across the band, which is approximately correct [Turneaure 2002a]. The as-built thickness of the photodetectors is 160 μm [Goebel 2003a]. The appropriate thickness for the calculation is 320 μm because the back side of the photodetector is a mirror and the photons enter the photodetector at angles that are approximately normal to the photodetector surface. The result is $k_{QE} = (dQ_c/dT)/Q_c = 2.9 \times 10^{-4}$ /K.

We assume a worst-case matching factor r_{QE} of 0.1 since the photodetectors are produced on the same substrate using the same material and processes, and they are in close proximity. Using Eqn 4-27, Eqn 4-28, and the maximum expected value of b of 2.29×10^3 marcsec, the angular bias variations $\Delta\theta_{b,QE}$ introduced by temperature variations in the quantum efficiency of the photodetectors are given by the following equation.

$$\Delta\theta_{b,QE} = 1.6 \times 10^{-10}\ \Delta T_{DMA} \qquad (4\text{-}31)$$

4.2.1.3 Charge Locked Loop

The only component that has any significant differential gain variation in the charge locked loop (CLL) is the feedback capacitor since the CLL amplifier acts as an error amplifier, has high gain, and its gain is relatively temperature insensitive. Differential variation in the feedback capacitance depends on the temperature coefficient of the fractional capacitance for the feedback capacitors k_{FB}, their temperature variations ΔT_{DMA}, and a matching factor r_{FB}. The differential gain variation is expressed by the following equation.

$$2\,\delta_{FB} = k_{FB}\; r_{FB}\; \Delta T_{DMA} \tag{4-32}$$

The feedback capacitors were manufactured by Electro Films, Inc. (now Vishay Electro-Films) and ordered as part number UNCA-129-5000-DL. The Si is doped so that it is conducting and its surface acts as one side of the capacitor. A SiO_x dielectric layer is grown on the Si substrate followed by a layer of metal, which acts as the other side of the capacitor. The capacitors were made from a single Si wafer, which was subsequently diced. The average capacitance of the batch is 0.590 pF. These capacitors are specified to have a temperature coefficient of +15 ppm/K ± 25 ppm/K over the temperature range from -55 C to +150 C [Vishay 2001]. Capacitance measurements at 6 K give an average value of 0.67 pF for 20 capacitors, but there could be a parasitic capacitance of as much as 0.1 pF [Goebel 2003b]. These measurements indicate that the conduction carriers of the doped Si do not freeze out and that there is no unusual behavior in the temperature dependence of the capacitance. According to the specification, the worst-case temperature coefficient of the fractional capacitance is 40 ppm/K (4×10^{-5} /K) in the above mentioned temperature range. We assume a very conservative value of 4×10^{-4} /K at the 72 K operating temperature since we lack experimental data at this temperature. Goebel estimates that the temperature coefficient of the fractional capacitance is less than 100 ppm/K [Goebel 2003b]. We assume a conservative worst-case matching factor r_{FB} of 0.1 because the two feedback capacitors for the plus/minus sides were produced adjacent to each other on the Si wafer and they are mounted on the same DMA high thermal conductivity sapphire substrate. Using Eqn 4-32 and the maximum expected value of b of 2.29×10^{3} marcsec, the bias variations $\Delta\theta_{b,FB}$ introduced by temperature variations of the feedback capacitors are given by the following equation.

$$\Delta\theta_{b,FB} = 2.2 \times 10^{-10}\; \Delta T_{DMA} \tag{4-33}$$

4.2.1.4 Conditioning Electronics

Farley [Farley 2003b] measured the thermally induced differential gain variation resulting from changes in TRE box temperature ΔT_{TRE} over the range -40 C < T_{TRE} < 60 C. The measurements give a temperature coefficient of fractional differential gain $d(2\delta)/dT$ of 12 ppm per K of TRE box temperature variation. This measured value is consistent with and substantially smaller than the worst-case value one calculates based on the temperature coefficients of the resistors that determine the gain of the conditioning electronics. The measured coefficient of 12 ppm/K leads to the following equation for angular bias $\Delta\theta_{b,CE}$.

$$\Delta\theta_{b,CE} = 0.7 \times 10^{-10}\; \Delta T_{TRE} \tag{4-34}$$

4.2.1.5 Digital Electronics

The voltage ramps for the plus and minus channels are both sampled at 2200 Hz by the same 16 bit analog to digital converter ADC resulting in a negligible dependence of the differential gain between them. Further the ADC employs a voltage reference with a very low temperature coefficient. For these reasons, any bias variations due to the digital electronics are negligible.

4.2.1.6 Summary

The total worst-on-worst angular bias temperature dependence $\Delta\theta_{b,R}$ for the processing of the plus and minus beams from the roof prism through the ADC is summarized by the following equation.

$$\Delta\theta_{b,R} = 3.8\times10^{-10}\ \Delta T_{DMA} + 0.7\times10^{-10}\ \Delta T_{TRE} \qquad (4\text{-}35)$$

4.2.2 Bias Variations at Roll Frequency

From Table 3-6 and Table 3-7, the worst-case amplitude for temperature variation of the DMA at roll frequency is 0.013 K, and from Table 3-5 the worst-case amplitude for temperature variation of the TRE at roll frequency is 0.0105 K. These values yield a worst-case amplitude of the angular bias at roll frequency of 5.7×10^{-12} rad or 0.0012 marcsec. Assuming the worst-case phase and amplitude changes of this bias with time yields an amplitude modulation of the roll frequency bias at both orbital and annual frequencies of 0.0012 marcsec, and a linear drift in the roll frequency bias of 0.0024 marcsec/yr. These results are listed in Table 4-12.

Table 4-12. Readout contributions to roll-frequency bias variations

Requirement	Title	Worst-Case Value
T003: 7.6.2.1	Linear Variation	0.0024 marcsec/yr
T003: 7.6.2.2	Annual Variation	0.0012 marcsec
T003: 7.6.2.3	Orbital Variation	0.0012 marcsec

4.2.3 Body- Fixed Bias Variations

From Table 3-6 and Table 3-7, the worst-case temperature variations of the DMA are an amplitude of 1.54 K at annual frequency and a linear drift rate of 0.74 K/yr. From Table 3-5, the worst-case temperature variations of the TRE are an amplitude of 8.7 K at annual frequency and a linear drift of 4.2 K/yr. These values yield a worst-case amplitude of the angular bias at annual frequency of 1.19×10^{-9} rad or 0.25 marcsec and a worst-case linear drift rate of 5.8×10^{-10} rad/yr or 0.12 marcsec/yr. The amplitude of 0.25 marcsec amplitude at annual frequency applies to all other frequencies in the body-fixed frame as a worst-case estimate. These results are listed in Table 4-13.

Table 4-13. Telescope readout contributions to body-fixed bias variations

Requirement	Title	Worst-Case Value
T003: 7.6.2.4	Linear Drift	0.12 marcsec/yr
T003: 7.6.2.5	Bias Variation at Other Frequencies	0.25 marcsec

4.3 Total Worst-on-Worst Error

This section provides the worst-case errors for the seven requirements. The bias variations are dominated by those coming from the imaging optics.

4.3.1 Roll-Frequency Angular Bias Requirements

Table 4-14 lists the three roll-frequency angular bias requirements, their specified values, and the worst-on-worst errors from Table 4-4, Table 4-9, and Table 4-12. The analysis shows that these requirements are met.

Table 4-14. Worst-on-worst error for roll-frequency bias variations

Requirement	Title	Required Value	Worst-on-Worst Case Value
T003: 7.6.2.1	Linear Variation	< 0.1 marcsec/yr over 1 yr	0.058 marcsec/yr over 1 yr
T003: 7.6.2.2	Annual Variation	< 0.4 marcsec over 1 yr	0.029 marcsec over 1 yr
T003: 7.6.2.3	Orbital Variation	< 0.1 marcsec over 1 yr	0.029 marcsec over 1 yr

4.3.2 Body-Fixed Angular Bias Requirements

Table 4-15 lists the two body-fixed angular requirements, their specified values, and the worst-on-worst errors from Table 4-5, Table 4-10, and Table 4-13. The analysis shows that these requirements are met.

Table 4-15. Worst-on-worst error for body-fixed bias variations

Requirement	Title	Required Value	Worst-Case Value
T003: 7.6.2.4	Linear Drift	1000 marcsec/yr over 1 yr	51 marcsec/yr over 1 yr
T003: 7.6.2.5	Bias Variation at Other Frequencies	1000 marcsec over 1 yr	7.4 marcsec over 1 yr

4.3.3 Scale-Factor Requirements

Table 4-16 lists the two scale-factor requirements, their specified values, and the worst-on-worst errors from Table 4-3 and Table 4-8. The analysis shows that these requirements are met.

Table 4-16. Worst-on-worst error for scale factor requirements

Requirement	Title	Required Value	Worst-on-Worst Case Value
T003-7.6.3.1	Orbital Frequency Scale Factor Variation	< 2 % (amplitude) over 1 week	0.49 % (amplitude) over 1 week
T003-7.6.3.2	Linear Drift in Telescope Scale Factor	< 2 %/day over 1 day	0.07 %/day over 1 day

References

[Analog Devices 2000a] Analog Devices, Data sheet for low power, high precision operational amplifier OP-97, undated, 2000.

[Analog Devices 200b] Analog Devices, Data sheet for high precision reference AD780, Rev. B, 2000.

[Analog Devices 2002] Analog Devices, Data sheet for 5 V precision reference/temperature transducer REF02, Rev. C, 2002.

[Bernier 2002] R. T. Bernier. Acworth, J. P. Turneaure, D. DeBra, "Flight Telescope/Window System Verification", GP-B Science Document S0570, 3 Mar 2002.

[Burns 1998] K. M. Burns, "Thermal Analysis of FEE Electronic Boxes, Connectors, and Tophat", EM No. TCS 332A, Lockheed Martin Missiles and Space Co., 13 Aug 1998.

[Burns 2002] K. M. Burns, "Correlation of SMD/Probe C thermal model with test data and projection of lifetime", EM No. TCS 342 B, Lockheed Martin Space Systems Co., 11 January 2002.

[Burch 1965] D. A. Burch, *J. Opt. Soc. Amer.*, **55**, p. 625 (1965).

[D'Ans 1962] J. D'Ans, *et al.*, *Zahlenwerte un funktionen aus physic, chemie astronomie, geophysik, und tecnik, sechsted auglage, II. Band Eigenschaften der materie in ihren aggregregatzustanden, 8. Teil Optische konstanten* (Springer-Verlag, Berlin, 1962) pp 3-492 to 3-495.

[Farley 2001a] R. P. Farley, "Telescope thermal requirements verification", GP-B Science Document S0558 Rev. -, 11 Oct 2001.

[Farley 2001b] R. P. Farley, "Procedure for TRE heater operation", as run procedure P0871, 3 Aug 2001.

[Farley 2003a] R. P. Farley, The sensitivity of the Southampton silicon diode temperature sensor is 602 K/V based on the supplied calibration data, Lockheed Martin Missiles and Space Co., private comm.., 2003.

[Farley 2003b] R. P. Farley, Analysis of data for TRE box during box level thermal vacuum testing, private comm., 2003.

[Goebel 2003a] J. H. Goebel, Ames Research Center, NASA, private comm., 2003.

[Goebel 2003b] J. H. Goebel, "Temperature dependence of the TRE feedback capacitor", S0829 Rev. -, 12 Mar 2003.

[Hall 1954] L. H. Hall, J. Bardeen, F. J. Blatt, "Infrared absorption spectrum of germanium", *Phys. Rev.* **96,** p. 559 (1954).

[Harris 1994] Harris Semiconductors, Technical data sheet for HS-565ARH high speed monolithic digital-to-analog converter, Nov 1994.

[Kirschenbaum 2002] "System design and documentation: Control system error budgets and capability", SCSE-04, Part 5 Rev. C (see Table 6.5-1), Lockheed Martin Space Systems Co., 18 Oct 2002.

[Koç 1997] M. Koç, "The characteristics of the temperature sense diode", GP-B Science Document S0772, 19 Aug 1997.

[Lockheed 1995] Lockheed Martin Space Systems Co., "Substrate, Window #4", Drawing 1C34165, 5 Apr 1995.

[Lockheed 1996] Lockheed Martin Space Systems Co., "Coated substrate, Window 1-3", Drawing 1C34170, 24 Jan 1996.

[Lockheed 1998] Lockheed Martin Missiles and Space Systems Co., "TRE analog board schematic diagram", Drawing 8A00851, 23 Jun 1998.

[Malitson 1962] L. H. Malitson, *J. Opt. Soc. Amer.* **52**, pp , 1962.

[Muhlfelder 2001] "QBS Thermal Stability", S0538 Rev. -, 12 Oct 2001.

[Phillips 1981] W. A. Phillips, ed., *Amorphous solids, low-temperature properties* (Springer-Verlag, Berlin, 1981) p. 92.

[Rajkanan 1979] K. Rajkanan, R. Singh, J. Shewchun, "Absorption coefficient for silicon solar cell calculations", *Solid State Elect.* **22**, pp. 793-795 (1979).

[Touloukian 1970a] Y. S. Touloukian, R. W. Powell, C. Y. Ho, P. G. Klemens, *Thermophysical Properties of Matter, Vol. 2 Thermal Conductivity of Nonmetallic Solids*, (Plenum, N.Y., 1970) pp. 183-193, 1970. The recommended thermal conductivity for fused quartz is found on page 193.

[Touloukian 1970b] Y. S. Touloukian, E. H. Buyer, *Thermophysical Properties of Matter, Vol. 5 Specific Heat of, Nonmetallic Solids*, (Plenum, N.Y., 1970) pp. 202-206, 1970b. We used the fused-quartz specific heat data of curve 6 found on page 205.

[Touloukian 1977] Y. S. Touloukian, R. K. Kirby, R. E. Taylor, T. Y. R. Lee, *Thermophysical Properties of Matter, Vol. 13, Thermal Expansion of Nonmetallic Solids*, (Plenum, N.Y., 1977) pp. 359-371, 1977. We used the thermal expansion data for curve 89 on page 369 to derive a temperature dependent thermal expansion coefficient.

[Turneaure 2002a] J. P. Turneaure, M. Heifetz, "Flight telescope/window system analyses of Wavelength Dependent Properties", GP-B Science Document S0619, 6 Mar 2002.

[Turneaure 2002b] J. P. Turneaure, "Verification of telescope readout linearity requirements", GP-B Science Document S0686, 3 Nov 2002.

[Vishay 2001] Vishay Electro-Films, Specifications for NC series thin film single value chip capacitors, Document Number 61033, Revision 07 Aug 2001.

[Wedel 1998] R. K. Wedel, "Updated thermal analyses of GP-B windows", Lockheed Martin Missiles and Space Co., EM No. TCS 217, 27 Jan 1998.

[Whelan 2002] R. Whelan, "SQUID readout electronics (SRE) specification", paragraph 3.2.3.1.2.5, Lockheed Martin Missile and Space Co. document P480136 Rev. D, 14 Mar 2002.

[Yang 2001] D. Yang, M. E. Thomas, S. G. Kaplan, et al., "Measurement of the infrared refractive index of sapphire as a function of temperature", *SPIE Aerosense*, 2001.

Appendix 1. Listing of *Mathematica*® notebook that calculates some telescope properties by ray tracing

Ray Trace of GP-B Flight Telescope

John P. Turneaure
25 March 2003

This notebook traces a pair of rays through the telescope to determine the {x, z} focal location. Using this ray tracing formalism, the following quantities are calculated.

1. The effective focal length of the telescope.
2. The z-position shift of focus, expressed as a derivative, due to a small change in the length of the metering tube.
3. The z-position shift of focus, expressed as a derivative, due to a small change in the radius of the secondary mirror.
4. The angular shift due to the bending of the metering tube.

Initial Definitions

Turn off spelling warnings.

```
Off[General::"spell", General::"spell1"];
```

The z position of the ray is with respect to the front plate surface in contact with the metering tube. The positive z direction is toward the guide star. Define the following quantities, which are in units of mm.

lm = length of metering tube from baseplate to front plate

rp = radius of the primary mirror,concave (neg)

rs = radius of the secondary mirror,convex (pos)

rt = radius of the tertiary mirror,convex (pos)

tp = thickness of primary mirror on axis

ts = thickness of secondary mirror on axis

tt = thickness of tertiary mirror on axis

Place numerical values for the telescope parameters in the list **vars**.

$$\text{vars} = \{\text{lm} \to \left(13 + \frac{660}{1000}\right)\left(25 + \frac{4}{10}\right),\ \text{rp} \to -\left(47 + \frac{477}{1000}\right)\left(25 + \frac{4}{10}\right),\ \text{rs} \to \left(91 + \frac{202}{1000}\right)\left(25 + \frac{4}{10}\right),\ \text{rt} \to \left(7 + \frac{484}{1000}\right)\left(25 + \frac{4}{10}\right),\ \text{tp} \to 1\left(25 + \frac{4}{10}\right),\ \text{ts} \to \frac{365}{1000}\left(25 + \frac{4}{10}\right),\ \text{tt} \to \frac{915}{1000}\left(25 + \frac{4}{10}\right)\};$$

Define number of digits to be used in calculations nc.

```
nc = 20;
```

Define Functions

Define function that returns the angle of the perpendicular to a mirror relative to its axis at an off axis position **x** and for a spherical mirror with radius **r**.

$$\alpha[x\_,\ r\_] := \mathrm{ArcSin}\left[\frac{x}{r}\right];$$

Define function that returns the angle of the perpendicular to the aspheric primary mirror relative to its axis at an off axis position x. This form includes the elliptic correction.

$$\alpha p[x\_] := \mathrm{ArcTan}\left[\frac{-x}{\sqrt{rp^2 - \left(1 - \frac{5849}{10000}\right) x^2}}\right];$$

Define function that returns the thickness of a spherical mirror at an off-axis position **x** and for a spherical mirror with a radius **r**, and a thickness at its center of **t**.

$$tx[x\_,\ r\_,\ t\_] := t - r\left(1 - \sqrt{\left(1 - \frac{x^2}{r^2}\right)}\right);$$

Define function that returns the thickness of the primary mirror at an off-axis position **x**.

$$txp[x\_] := tp - \frac{x^2}{rp}\ \frac{1}{1 + \sqrt{1 - \frac{x^2}{rp^2}\left(1 - \frac{5849}{10000}\right)}};$$

Define function that returns the angle γ of a reflected ray with respect to the telescope axis for an incident ray at angle β with respect to the telescope axis after encountering a spherical mirror at a off-axis position **x**, and with a spherical radius **r**.

$$\gamma[x\_,\ r\_,\ \beta\_] := \beta + 2\alpha[x,\ r];$$

Define function that returns the angle γ**p** of a reflected ray with respect to the telescope axis for an incident ray at angle β with respect to the telescope axis after encountering the primary mirror at an off-axis position **x**.

$$\gamma p[x\_,\ \beta\_] := \beta + 2\alpha p[x];$$

Define function that sorts out the form of the solution **rslt** and returns the proper values of **x** and **z**. This function assumes that there are at most two solutions in **rslt**. The parameter **s** is 1 for the primary and tertiary mirrors and is 0 for the secondary mirror.

```
find[rslt_, x_, z_, s_] := Module[{lcnt, nxs, nzs},
  If[rslt[[1, 1, 1]] === x, nxs = 1; nzs = 2, nxs = 2; nzs = 1];
  If[Length[rslt] == 2,
   If[s == 0, If[rslt[[1, nzs, 2]] < rslt[[2, nzs, 2]], lcnt = 1, lcnt = 2],
    If[rslt[[1, nzs, 2]] > rslt[[2, nzs, 2]], lcnt = 1, lcnt = 2]],
   lcnt = 1];
  x = N[rslt[[lcnt, nxs, 2]], nc];
  z = N[rslt[[lcnt, nzs, 2]], nc];
  Remove[lcnt, nxs, nzs]]
```

Define function that returns the value of {**xo, zo,** β**o**} given the parameters {**xi, zi,** β**i**}, **Δlm**, **lPnt**, and the properties of the telescope. The vector {**xi, zi,** β**i**} is the initial position and direction of a ray as it enters the telescope. The variable **Δlm** is a small change in the length of the metering tube from the nominal value of **lm**. The logical value **lPnt** causes some values to print if it is True and not if it is False. The vector {**xo, zo,** $\boldsymbol{\beta}$**o**} is the position and direction of a ray as it leaves the primary mirror.

```
funcP[xi_, βi_, Δlm_, xo_, zo_, βo_, lPnt_] :=
 Module[{eqn1, eqn2, rslt},
  eqn1 = zo == -(lm + Δlm) + txp[xo];
  eqn2 = xo == xi;
  rslt = Solve[{eqn1, eqn2}, {xo, zo}] /. vars;
  find[rslt, xo, zo, 1];
  βo = N[γp[xo, βi] /. vars, nc];
  If[lPnt,
   Print["    x = ", N[xo], "   z = ", N[zo], "   β = ", N[βo]]];
  Remove[eqn1, eqn2, rslt]]
```

Define function that returns the value of {**xo, zo,** $\boldsymbol{\beta}$**o**} given the parameters {**xi, zi,** $\boldsymbol{\beta}$**i**}, **Δxs**, **Δ**$\boldsymbol{\alpha}$**s**, **rsA**, **lPnt**, and the properties of the telescope. The vector {**xi, zi,** $\boldsymbol{\beta}$**i**} is the position and direction of a ray as where it leaves the primary mirror. The variable **Δxs** is a shift in the transverse position of the secondary mirror. The variable **Δ**$\boldsymbol{\alpha}$**s** is a small change in the angle of the secondary mirror axis relative to the primary mirror axis. The variable **rsA** is the shifted spherical radius of the secondary mirror. The logical value **lPnt** causes some values to print if it is True and not if it is False. The vector {**xo, zo,** $\boldsymbol{\beta}$**o**} is the position and direction of a ray as it leaves the secondary mirror.

```
funcS[xi_, zi_, βi_, Δxs_, Δαs_, rsA_, xo_, zo_, βo_, lPnt_] :=
 Module[{eqn1, eqn2, rslt},
  (* Correct position for Δxs and Δαs *)
  eqn1 = zo == -tx[xo - Δxs, rsA, ts] - (xo - Δxs) Tan[Δαs];
  eqn2 = xo == xi + (zo - zi) Tan[βi];
  rslt = Solve[{eqn1, eqn2}, {xo, zo}] /. vars;
  find[rslt, xo, zo, 0];
  (* Correct angle for Δαs and Δxs *)
  βo = N[(γ[xo - Δxs, rsA, βi] - 2 Δαs) /. vars, nc];
  If[lPnt,
   Print["    x = ", N[xo], "   z = ", N[zo], "   β = ", N[βo]]];
  Remove[eqn1, eqn2, rslt]]
```

Define function that returns the value of {**xo, zo,** $\boldsymbol{\beta}$**o**} given the parameters {**xi, zi,** $\boldsymbol{\beta}$**i**}, **Δlm**, **lPnt**, and the properties of the telescope. The vector {**xi, zi,** $\boldsymbol{\beta}$**i**} is the position and direction of a ray as it leaves the secondary mirror. The variable **Δlm** is a small change in the length of the metering tube from the nominal value of **lm**. The logical value **lPnt** causes some values to print if it is True and not if it is False. The vector {**xo zo,** $\boldsymbol{\beta}$**o**} is the position and direction of a ray as where it leaves the tertiary mirror.

```
funcT[xi_, zi_, βi_, Δlm_, xo_, zo_, βo_, lPnt_] :=
 Module[{eqn1, eqn2, rslt},
  eqn1 = zo == -(lm + Δlm) + tx[xo, rt, tt];
  eqn2 = xo == xi - (zo - zi) Tan[βi];
  rslt = Solve[{eqn1, eqn2}, {xo, zo}] /. vars;
  If[rslt[[1, 1, 1]] === xo, nxt = 1; nzt = 2, nxt = 2; nzt = 1];
  find[rslt, xo, zo, 1];
  βo = N[γ[xo, rt, βi] /. vars, nc];
  If[lPnt,
   Print["    x = ", N[xo], "   z = ", N[zo], "   β = ", N[βo]]];
  Remove[eqn1, eqn2, rslt]]
```

Define a function that finds the focal postion {**xo, zo**} given the parameters {**xi, zi,** $\boldsymbol{\beta}$**i**}, {**x0i,z0i,** $\boldsymbol{\beta}$**0i**}, and **lPnt**. The logical value **lPnt** causes some values to print if it is True and not if it is False. The focal position is the intersction of two rays {**xi, zi, βi**} and {**x0i,z0i, β0i**} leaving the tertiary mirror. The vector {**xo, zo**} is the longitudinal and transverse focal position.

```
funcF[xi_, zi_, βi_, x0i_, z0i_, β0i_, xo_, zo_, lPnt_] :=
 Module[{eqn1, eqn2, rslt, nxf, nzf},
  eqn1 = xo == xi + (zo - zi) Tan[βi];
  eqn2 = xo == x0i + (zo - z0i) Tan[β0i];
  rslt = Solve[{eqn1, eqn2}, {xo, zo}] /. vars;
  If[rslt[[1, 1, 1]] === xo, nxf = 1; nzf = 2, nxf = 2; nzf = 1];
  xo = N[rslt[[1, nxf, 2]], nc];
  zo = N[rslt[[1, nzf, 2]], nc];
  If[lPnt, Print["     x = ", Chop[N[xo]], "  z = ", N[zo]]];
  Remove[eqn1, eqn2, rslt, nxf, nzf]]
```

Define function that returns the focal position {**xo, zo**} relative to the aft side of the front plate and the axis of the primary mirror given **Δlm**, **rsA**, **x0**, **β0**, **Δαs**, **Δxs** and **lPnt**. The function **Δf** returns the z-postion of the focal position as well as asigning the values of **xo** and **zo**.

Δlm = Δ length of metering tube with respect to standard length **lm** (mm)

rsA = radius of secondary mirror after including small change from **rs** (mm)

x0 = initial x position of ray at surface of primary mirror (mm)

β0 = initial direction of ray (rad)

Δαs = angle at which secondary mirror is tilted with respect to primary mirror axis (rad). A positive angle corresponds to the outer normal to mirror surface on its axis (-Z direction) moving in the -X direction.

Δxs = transverse offset of the axis of the secondary mirror with respect to the primary mirror axis (mm). A positive Δxs is in the direction of the +X axis.

lPnt = logical variable; if TRUE it causes values to be printed during evaluation of Δf

```
Δf[Δlm_, rsA_, x0_, β0_, Δαs_, Δxs_, lPnt_] :=
 Module[{eqn1, eqn2, rslt, z0p, zp, β0p, βp, β0s, βs, β0t, βt},
  (* FIRST STEP: Find position and angle after
      reflection from primary mirror for incident
      ray parallel to axis at radial position x. *)
  If[lPnt, Print["PRIMARY MIRROR"]];
  (* Off-axis ray *)
  If[lPnt, Print["  Off-axis ray"]]; Clear[xp, zp];
  funcP[x0, β0, Δlm, xp, zp, βp, lPnt];
  (* On-axis ray *)
  If[lPnt, Print["  On-axis ray"]]; Clear[x0p, z0p];
  funcP[0, β0, Δlm, x0p, z0p, β0p, lPnt];
  (* SECOND STEP: Find x and z position where ray intersects
      secondary mirror and resulting angle of reflected ray. *)
  If[lPnt, Print["SECONDARY MIRROR"]];
  (* Off-axis ray *)
  If[lPnt, Print["  Off-axis ray"]]; Clear[xs, zs];
  funcS[xp, zp, βp, Δxs, Δαs, rsA, xs, zs, βs, lPnt];
  (* On-axis ray *)
  If[lPnt, Print["  On-axis ray"]]; Clear[x0s, z0s];
  funcS[x0p, z0p, β0p, Δxs, Δαs, rsA, x0s, z0s, β0s, lPnt];
  (* THIRD STEP: Find x and z position where ray intersects
      tertiary mirror and resulting angle of reflected ray. *)
  If[lPnt, Print["TERTIARY MIRROR"]];
  (* Off-axis ray *)
  If[lPnt, Print["  Off-axis ray"]]; Clear[xt, zt];
  funcT[xs, zs, βs, Δlm, xt, zt, βt, lPnt];
  (* On-axis ray *)
  If[lPnt, Print["  On-axis ray"]]; Clear[x0t, z0t];
  funcT[x0s, z0s, β0s, Δlm, x0t, z0t, β0t, lPnt];
  (* FOURTH
    STEP: Find z postion where ray intersects the telescope axis *)
  If[lPnt, Print["FOCAL LOCATION"]]; Clear[xf, zf];
  funcF[xt, zt, βt, x0t, z0t, β0t, xf, zf, lPnt];
  zf]
```

Calculate focal position for nominal lm and rs with xp equal to 5.0 mm.

```
Δf[0, rs, 5, 0, 0, 0, True];

PRIMARY  MIRROR

  Off-axis  ray

    x = 5.    z = -321.554    β = -0.00829243

  On-axis  ray

    x = 0.    z = -321.564    β = 0.

SECONDARY  MIRROR

  Off-axis  ray

    x = 2.41035    z = -9.26975    β = -0.00621144

  On-axis  ray

    x = 0.    z = -9.271    β = 0.

TERTIARY  MIRROR

  Off-axis  ray
```

```
x = 0.457111    z = -323.724    β = -0.0014021
```

```
On-axis ray
```

```
x = 0.    z = -323.723    β = 0.
```

```
FOCAL LOCATION
```

```
x = 0  z = 2.29486
```

Calculate Focal Length of Telescope

Calculate the focal length **f**.

```
Δf[0, rs, 1, 0, 0, 0, False];
xf0 = xf;
Δf[0, rs, 1, π/(180 3600), 0, 0, False];
xf1 = xf;
(* Δxf is the transverse shift in the focal
  position due to a 1 arcsec change in the wavefront *)
Δxf = xf1 - xf0;
f = Δxf / Sin[π/(180 3600)];
Print["Focal Length = ", f, " mm"];
```

```
Focal Length = 3566.04402896550 mm
```

Calculate Angle Error Due to Bending of the Metering Tube

The calculation is done for the following parameter values which correspond to 1 microwatt.

> $\Delta\alpha\mathbf{s}$ = 6.33 × 10^{-11} rad (angular tilt of secondary mirror with respect to primary mirror axis)
>
> **Δxs** = 1.10 × 10^{-8} mm (transverse position shift of the secondary center with respect to primary axis)

Calculate transverse focal position shift **Δxf** with respect to the primary mirror axis.

```
Δαs = 6.33×10^-11;
Δxs = 1.10×10^-8;
Δf[0, rs, 1, 0, Δαs, Δxs, False];
Print[xf];
```

```
-2.33959 × 10^-7
```

Calculate equivalent angle $\Delta\beta$ for this shift.

```
Δβ = ArcSin[(Δxs - xf)/f];
Print["Angle Shift = ", Δβ, " rad"];
Print["Angle Shift = ", (180 3600 10^3)/π Δβ, " marcsec"];
```

```
Angle Shift = 6.86922 × 10^-11 rad
```

```
Angle Shift = 0.0141688 marcsec
```

Calculate Derivative of Δf with Respect to Δlm and to the % change in rs.

Calculate the value of **ΔfΔlm**, which is the derivative of **Δf** with respect to **Δlm**.

```
ΔfΔlm = (Δf[1/100, rs, 0.1, 0, 0, 0, False] - Δf[0, rs, 0.1, 0, 0, 0, False]) / (1/100);
Print["ΔfΔlm = ", N[ΔfΔlm], " mm/mm"];
Print["ΔfΔlm = ", N[0.0254 ΔfΔlm], " mm/milli-inch"];
```

```
ΔfΔlm = -55.5328 mm/mm
```

```
ΔfΔlm = -1.41053 mm/milli-inch
```

Calculate the value of **ΔfΔrs**, which is the derivative of **Δf** with respect to the percent change in **rs**.

```
ΔfΔrs = 1/(1/1000) (Δf[0, (1 + 1/100000) rs, 0.1, 0, 0, 0, False] -
     Δf[0, rs, 0.1, 0, 0, 0, False]);
Print["ΔfΔrs = ", N[ΔfΔrs], " mm/%"];
```

```
ΔfΔrs = -25.512 mm/%
```

Change in Focal Position for a Diverging 1 Wave De-Collimation of the Incident Wave with Wavelength of 668 nm.

Define the following symbols and use SI units.

λ = wavelength of light

d = diameter of telescope aperture

One wavelength of de-collimation corresponds to spherical wave incident on the primary mirror with one wavelength variation across the aperture of the telescope (i.e. the active diameter of the primary mirror).

Find the radius **rL** corresponding to the spherical wave.

```
Clear[rL];
vars1 = {λ → 700 10^-9, d → (5 + 66/100) 254/10000};
eqn = λ == rL (1 - Sqrt[1 - (d/(2 rL))^2]);
rslt = Solve[eqn, rL] /. vars1;
rL = 10^3 rslt[[1, 1, 2]];
Print["Radius corresponding to 1 wave of defocus = ", N[rL], " mm"];
```

```
Radius corresponding to 1 wave of defocus = 3.69073 × 10^6 mm
```

Find change in focal position **Δf** (in mm) for a 1 wave de-collimation.

```
eqn = Δf == Together[( f rL1 / (rL1 - f) ) - f];
rslt = Solve[eqn, Δf] /. vars1 /. rL1 → rL;
Δf = rslt[[1, 1, 2]];
Print[
  "Shift in focal position for 1 wave of defocus = ", N[Δf], " mm"];
```

```
Shift in focal position for 1 wave of defocus = 3.4489 mm
```

Derivative of Waves of Defocus with Respect to Δlm and % Change in Radius of Secondary Mirror

Find derivative **ΔnΔlm** of waves of defocus with respect to **Δlm**.

```
Print["ΔnΔlm = ", N[-ΔfΔlm / Δf], " waves/mm"];
Print["ΔnΔlm = ", N[-(254/10000) ΔfΔlm / Δf], " waves/milli-inch"];
```

```
ΔnΔlm = 16.1016 waves/mm

ΔnΔlm = 0.40898 waves/milli-inch
```

Find derivative **ΔnΔrs** of waves of defocus with respect to % change in **rs**.

```
Print["ΔnΔrs = ", N[-ΔfΔrs / Δf], " waves/%"];
```

```
ΔnΔrs = 7.39713 waves/%
```

Appendix 2. Listing of *Mathematica*® notebook that calculates the thermal properties of the telescope that effect defocus and angular bias changes

---

Thermal Model for Telescope

John P. Turneaure
March 27, 2003

This *Mathematica* notebook provides calculations related to the thermal properties and thermal loads on the telescope. The following calculations are made.

HEAT POWER FLOW

1. **p0** The heat power flow when the telescope forward plate is at 6 K and the telescope baseplate is at 2.5 K.

METERING TUBE QUANTITIES

2. **Δlmtp0** The length change in the telescope metering tube due to longitudinal heat power flow **p0**.
3. **Δnmtp0** The defocus change in waves due to **Δlmtp0**.
4. **ΔlmtΔp** The derivative of the metering tube length change with respect to heat power at a nominal heat power flow of **p0**.
5. **ΔnmtΔp** The derivative of the defocus change in waves with respect to heat power at a nominal heat power flow of **p0** due to the metering tube length change.

SECONDARY MIRROR QUANTITIES

6. **Δrsp0** The percentage change in the spherical radius of the secondary mirror at a nominal heat power flow of **p0**.
7. **Δnrsp0** The defocus change in waves due to **Δrsp0**.
8. **ΔrsΔp** Percentage change in the spherical radius of the secondary mirror due to 0.25 mW heat power added to nominal heat power **p0**.
9. **ΔnrsΔp** The derivative of the defocus change in waves with respect to heat power due to a secondary mirror spherical radius change at a nominal heat power flow of **p0**.

COMBINED METERING TUBE AND SECONDARY MIRROR QUANTITIES

10. **ΔnΔp** The derivative of the defocus change in waves with respect to added heat power at a nominal heat power flow of **p0**.

11. **ΔbΔp** The derivative of the percentage change in scale factor **b** with respect to added heat power at a nominal heat power flow of **p0**.

Initial Definitions

Turn off warnings for spelling.

```
Off[General::"spell", General::"spell1"];
```

Load linear regression package.

```
<< Statistics`LinearRegression`
```

Define variables:

INPUT VARIABLES

lm = length of metering tube (mm)

iRm = inner radius of metering tube (mm)

oRm = outer radius of metering tube (mm)

rs = nominal radius of secondary mirror (mm)

dNdLM = number of waves per mm of change in metering tube length (waves/mm)

dNdRS = number of waves per percentage change in secondary mirror radius (waves/%)

dBdN = fractional scale factor change per wave of defocus (1/wave)

tf = temperature at forward end of metering tube (K)

ta = temperature at aft end of metering tube (K)

ΔLdata = list of thermal expansion data vs temperature

κdata = list of thermal conductivity data vs temperature

OUTPUT VARIABLES

p0 = nominal heat power flow from forward to aft end of metering tube (W)

α = temperature coefficient of expansion, which is function of temperature **tα** (1/K)

κ = thermal conduction, which is a function of temperature **tκ** (W/mm/K)

Δl = length change of metering tube, which is a function of heat power **p** (mm)

Δlmtp0 = metering tube length change of metering tube for heat power **p0** (mm)

Δnmtp0 = defocus change in waves due to metering tube for heat power **p0** (waves)

ΔlmtΔp = derivative of metering tube length with respect to heat power (mm/W)

ΔnmtΔp = derivative of defocus change due to metering tube length change with respect to added heat power (waves/W)

Δrsp0 = percentage change in secondary mirror radius due to heat power **p0** (%)

Δnrsp0 = defocus change from secondary mirror radius change due to heat power **p0** (waves)

tΔp = temperature of secondary mirror due to heat power of **p0** + 0.25 mW (K)

ΔrsΔp = percentage change in secondary mirror radius due to added heat power 0.25 mW (%)

ΔnrsΔp = derivative of defocus change from secondary mirror radius change with respect to added heat power (waves/W)

ΔnΔp = derivative of defocus change from both secondary mirror and metering tube with respect to added heat power (waves/W)

ΔbΔp = derivative of the percentage change in the scale factor **b** with respect to added heat power (%/W)

Establish values for input parameters.

```
vars = {lm → 13.660 25.4, iRm → (25.4 5.9)/2, oRm → (25.4 6.5)/2, rs → 91.202 25.4,
  dNdLM → 16.1, dNdRS → 7.40, dBdN → 0.67, tf → 6., ta → 2.5}
```

```
{lm → 346.964 , iRm → 74.93 , oRm → 82.55 , rs → 2316.53 ,
 dNdLM → 16.1 , dNdRS → 7.4 , dBdN → 0.67 , tf → 6., ta → 2.5}
```

Find Polynomial Form for Thermal Expansion and Conduction

Thermal Expansion

Define the following quantities:

ΔLdata = list that contains a temperature and a fractional length change with an arbitrary reference temperature

ΔLtmp = function giving the fractional length change as a function of temperature **t***α*

Use data from curve 89 from Touloukian (White).

```
ΔLdata =
  {{2.1, 0.0 10^-8}, {2.5, -0.3 10^-8}, {3.2, -0.8 10^-8}, {3.6, -1.4 10^-8},
   {4.0, -1.8 10^-8}, {4.2, -2.5 10^-8}, {5.1, -4.9 10^-8}, {5.6, -7.2 10^-8},
   {6.2, -10.6 10^-8}, {6.9, -16.2 10^-8}, {7.5, -22.9 10^-8}};
```

```
Regress[ΔLdata, {1, tα^2, tα^3}, tα]
```

```
ΔLtmp = Fit[ΔLdata, {1, tα^2, tα^3}, tα]
```

$-9.57032 \times 10^{-9} + 3.33855 \times 10^{-9}\, t\alpha^2 - 9.56677 \times 10^{-10}\, t\alpha^3$

```
α = D[ΔLtmp, tα]
```

$6.6771 \times 10^{-9}\ t\alpha - 2.87003 \times 10^{-9}\ t\alpha^2$

Thermal Conductivity

Define the following quantities:

κdata = list containing the temperature / thermal conductivity pairs

Use data from recommeneded curve in Touloukian. Units are in K and W/cm/K.

```
κdata = {{2.0, .00054}, {3., .0008}, {5.0, .00118},
  {6., .00124}, {8.0, 0.00126 }, {10., .00127}}
```

```
{{2., 0.00054 }, {3., 0.0008 }, {5., 0.00118 },
 {6., 0.00124 }, {8., 0.00126 }, {10., 0.00127 }}
```

```
Regress[κdata, {1, tκ^3}, tκ]
```

Divide by 10 to convert from W/cm/K to W/mm/K.

$$\kappa = \text{Simplify}\left[\frac{\text{Fit}[\kappa\text{data}, \{1, t\kappa^2\}, t\kappa]}{10}\right]$$

$0.0000800843 + 6.23926 \times 10^{-7}\ t\kappa^2$

Find Heat Power Flow For Nominal Conditions

Find the heat power flow for the nominal conditions are that forward end of the metering tube is at tf and the aft end is at ta.

$$p0 = \pi \frac{(\text{oRm}^2 - \text{iRm}^2)}{\text{lm}} \int_{ta}^{tf} \kappa \, d\, t\kappa \; /. \; \text{vars}$$

0.00349831

Metering Tube

Define Function That Gives The Metering Tube Length Change

$$\begin{aligned}
&\Delta l[p_] := \text{Module}[\{\text{eqn1}, \text{eqn2}, \beta\},\\
&\quad \text{eqn1} = \{z'[t\kappa] == \frac{\pi (\text{oRm}^2 - \text{iRm}^2)\, \kappa}{p} \; /. \; \text{vars},\ z[2.5] == 0.0\};\\
&\quad \text{eqn2} = z == \text{DSolve}[\text{eqn1}, z[t\kappa], t\kappa][[1, 1, 2]];\\
&\quad \beta = \alpha \; /. \; t\alpha \to \text{Solve}[\text{eqn2}, t\kappa][[3, 1, 2]];\\
&\quad \text{NIntegrate}[\beta, \{z, 0., \text{lm} \; /. \; \text{vars}\}]];
\end{aligned}$$

Length And Defocus Changes Due To p0

Calculate the length change of the metering tube due to the heat power p0 (mm).

```
Δlmtp0 = Δl[p0]
```

-9.52454×10^{-6}

Calculate the defocus change in waves for metering tube due to the heat power p0 (waves).

```
Δnmtp0 = Δlmtp0 dNdlM /. vars
```

```
-0.000153345
```

Δ Length And Δ Defocus Changes Due To Δp Heat Power Change From p0

The quantity **ΔlmtΔp** is the derivative of the metering tube length change with respect to heat power change assuming at the nominal temperature conditions (mm/W).

$$\Delta lmt\Delta p = \frac{\Delta l[p0 + 0.001] - \Delta l[p0]}{0.001}$$

```
-0.00375876
```

Derivative of defocus change in waves with respect to added heat power above the nominal value of p0 (waves/W).

```
ΔnmtΔp = dNdlM ΔlmtΔp /. vars
```

```
-0.0605161
```

Secondary Mirror

Changes Due To p0

Calculate percentage change in radius of secondary mirror due to p0 (%).

```
Δrsp0 = 100 ((α /. tα → tf) - (α /. tα → ta)) /. vars
```

-6.20136×10^{-6}

Calculate total change in waves due to p0 (waves).

```
Δnrsp0 = dNdRS Δrsp0 /. vars
```

```
-0.0000458901
```

Temperature Of Secondary Mirror Due To 0.25 mW Added Heat Power

Define equation relating the heat power to the lower and upper temperatures, the thermal conductivity, and the geometry of the metering tube.

$$eqn1 = p0\Delta p == \pi \frac{(oRm^2 - iRm^2)}{lm} \int_{ta}^{tu} \kappa \, d t\kappa \; /.\; vars$$

$$p0\Delta p == 10.8654\ (-0.00020346 + 0.0000800843\ tu + 2.07975 \times 10^{-7}\ tu^3)$$

Solve the equation for the temperature of the secondary mirror for a heat power of p0 + 0.25 mW.

```
tΔp = Solve[eqn1 /. p0Δp → p0 + 0.00025, {tu}][[3, 1, 2]]
```

```
6.22255
```

Derivative Of Defocus Change With Respect To Added Power

Calculate percentage change in radius of secondary mirror due to change from p0 of 0.25 mW.

```
ΔrsΔp = (100 ((α /. tα → tΔp) - (α /. tα → ta)) /. vars) - Δrsp0
```

```
-6.32075 ×10^-7
```

Calculate derivative of defocus change in waves with respect to added power (waves/W).

$$\Delta nrs\Delta p = \frac{dNdRS\,\Delta rs\Delta p}{0.00025} \;/.\; vars$$

```
-0.0187094
```

Metering Tube And Secondary Mirror

Calculate total derivative of defocus change in waves with respect to added heat power (waves/W).

```
ΔnΔp = ΔnmtΔp + ΔnrsΔp
```

```
-0.0792255
```

Find Derivative Of Percentage Change In Scale Factor With Respect To Added Power

```
ΔbΔp = 100 ΔnΔp dBdN /. vars
```

```
-5.30811
```

Appendix 3. Listing of *Mathematica*® notebook that calculates the worst-case variation in the thermal radiation incident of the telescope forward plate at roll and orbital frequencies

Thermal Radiation At Roll & Orbital Frequencies Reaching SIA

John P. Turneaure

March 25, 2003

This *Mathematica* notebook calculates the worst-case variation at roll and orbital frequencies of the thermal radiation down the probe neck that reaches the Science Instrument Assembly.
This calculation uses a very simple model. It assumes (1) the power flow reaching each of Windows #1 through #3 is modulated by the temperature modulation of window above it, (2) each window is at its equilibrium temperature but is thermally isolated except for the modulated thermal power input from above, and (3) the input modulation is due to a known temperature modulation of Window #4.

Initialization

Turn off spelling warnings.

```
Off[General::"spell", General::"spell1"];
```

Create lists of the window thermal properties. The Tn and Pn of the windows from the analysis by K. Burns, Engineering Memorandum TCS 342 B. The specific heat for fused quartz is from *Thermal Physical Properties of Matter, Nonmetallic Solids, Vol. 2*, Y. S. Touloukian, R. W. Powell, C. Y. Ho, P. G. Klemens (Plenum, N.Y., 1970) pp 183-193.

Tn[[n]] = Temperature of Window #n (K)

Pn[[n]] = Power absorbed by Window #n from above (W)

kn[[n]] = Specific heat of Window #n (J/g/K)

tn[[n]] = Temperature variation at roll or orbital frequency of Window #n (K)

pn[[n]] = Power variation reaching Window #n from above at roll or orbital frequency (W)

```
Tn = {28., 72., 129., 155.};
Pn = {.006, .058, .289};
kn = 1/4.186 {8.6 10^-3, 4.1 10^-2, 8.4 10^-2};
tn = Table[0, {i, 4}];
pn = Table[0, {i, 4}];
```

Mass of Window #1 through #3 in grams.

$$mW = \pi \left(\frac{6.5}{2}\right)^2 .65\, 2.54^3;$$

Heat capacity of Window #n in J/K.

```
Kn = mW kn;
```

Roll angular frequency in radians/s.

$$\omega r = \frac{2\pi}{180.};$$

Orbital angular frequency at roll in radians/s.

$$\omega O = \frac{2\pi}{97.5\, 60.};$$

Maximum thermal radiation power reaching the Science Instrument Assembly by radiation through the probe neck in W.

$$P0 = 10.\, 10^{-6};$$

Calculate temperature variations and power variations at roll frequency

Temperature variation of Window #4 is estimated to be 0.012 K from analysis by Burns.

```
tn[[4]] = 0.012;
```

Calculate p3. The form used here and below is based on the assumption that all of the power comes from the window above and is of the form σ T^4.

$$pn[[3]] = \frac{4\, Pn[[3]]\, tn[[4]]}{Tn[[4]]}$$

0.0000894968

Calculate t3. The form used here and below is based on the assumption that the window is thermally isolated, but remains on average at its equilibrium temperature.

$$tn[[3]] = \frac{pn[[3]]}{Kn[[3]]\, \omega r}$$

0.000361484

Calculate p2.

$$pn[[2]] = \frac{4\, Pn[[2]]\, tn[[3]]}{Tn[[3]]}$$

6.5011×10^{-7}

Calculate t2.

$$tn[[2]] = \frac{pn[[2]]}{Kn[[2]]\, \omega r}$$

5.37977×10^{-6}

Calculate p1.

$$pn[[1]] = \frac{4\, Pn[[1]]\, tn[[2]]}{Tn[[2]]}$$

1.79326×10^{-9}

Calculate t1.

$$tn[[1]] = \frac{pn[[1]]}{Kn[[1]]\,\omega r}$$

7.07465×10^{-6}

Calculate p0, which is the power variation at roll frequency reaching the Science Instrument Assembly.

$$p0 = \frac{4\,P0\,tn[[1]]}{Tn[[1]]}$$

1.01066×10^{-13}

Calculate temperature variations and power variations at orbital frequency

Temperature variation of Window #4 is estimated to be 0.25 K from analysis by Burns.

$tn[[4]] = 0.25;$

Calculate p3. The form used here and below is based on the assumption that all of the power comes from the window above and is of the form σ T^4.

$$pn[[3]] = \frac{4\,Pn[[3]]\,tn[[4]]}{Tn[[4]]}$$

0.00186452

Calculate t3. The form used here and below is based on the assumption that the window is thermally isolated, but remains on average at its equilibrium temperature.

$$tn[[3]] = \frac{pn[[3]]}{Kn[[3]]\,\omega o}$$

0.244755

Calculate p2.

$$pn[[2]] = \frac{4\,Pn[[2]]\,tn[[3]]}{Tn[[3]]}$$

0.000440179

Calculate t2.

$$tn[[2]] = \frac{pn[[2]]}{Kn[[2]]\,\omega o}$$

0.118383

Calculate p1.

$$pn[[1]] = \frac{4\,Pn[[1]]\,tn[[2]]}{Tn[[2]]}$$

0.000039461

Calculate t1.

$$tn[[1]] = \frac{pn[[1]]}{Kn[[1]]\,\omega o}$$

0.0505957

Calculate p0, which is the power variation at roll frequency reaching the Science Instrument Assembly.

$$p0 = \frac{4\,P0\,tn[[1]]}{Tn[[1]]}$$

7.22796×10^{-8}

Appendix 4. Listing of *Mathematica*® notebook that calculates temperature dependence of the relative quantum efficiency of the photodetectors

Temperature Coefficient of Quantum Efficiency

John P. Turneaure
March 25, 2003

This *Mathematica* notebook calculates the temperature coefficient of the fractional quantum efficiency based on the semi-empirical formalism of Rajkanan *et al.* (K. Rajkanan, R. Singh, J. Shewchun, "Absorption coefficient of silicon for solar cell calculations", *Solid State Electronics* 22 (1979), 791-795).

Initialization

Turn off spelling warnings.

```
Off[General::"spell", General::"spell1"];
```

Assign values from Rajkanan *et al.* to the following quantities.

eg10 = indirect gap 1 (ev)
eg20 = indirect gap 2 (ev)
egd = direct allowed gap (ev)
ep1 = Debye temperature 1 (ev)
ep2 = Debye temperature 2 (ev)
c1 = constant associated with ep1
c2 = constant associated with ep2
a1 = constant associated with eg1 (1/(cm eV^2)
a2 = constant associated with eg2 (1/(cm eV^2)
ad = constant associated withe egd (1/(cm eV^(1/2))
h = Plank's constant (eV s)
k = Boltzmann's constant (eV/K)
c = velocity of light (nm/s)
t = thickness of photodetector layer (μm)
λ = wavelength of photons (nm)
β = constant (eV/K)
γ = constant (K)

```
vars = {eg10 → 1.1557, eg20 → 2.5, egd → 3.2,
   ep1 → 1.827 10^-2, ep2 → 5.773 10^-2, c1 → 5.5, c2 → 4.0,
   a1 → 3.231 10^2, a2 → 7.237 10^3, ad → 1.052 10^6, h → 2 π 6.582 10^-16,
   k → 8.617 10^-5, c → 3.0 10^17, t → 160., β → 7.021 10^-4, γ → 1108.};
```

Define temperature dependent functions **eg1[T]** and **eg2[T]**.

```
eg1[T_] := (eg10 - β T^2/(T + γ)) /. vars;
eg2[T_] := (eg20 - β T^2/(T + γ)) /. vars;
```

Define the function α**[T,**λ**]** (1/μm), which is the inverse characteristic absorption distance.

```
α[T_, λ_] := 10^-4 (If[h c/λ + ep1 > eg1[T1], c1 a1 (h c/λ - eg1[T1] + ep1)^2/(Exp[ep1/(k T)] - 1), 0] +
    If[h c/λ + ep1 > eg2[T1], c1 a2 (h c/λ - eg2[T1] + ep1)^2/(Exp[ep1/(k T)] - 1), 0] +
    If[h c/λ + ep2 > eg1[T1], c2 a1 (h c/λ - eg1[T1] + ep2)^2/(Exp[ep2/(k T)] - 1), 0] +
    If[h c/λ + ep2 > eg2[T1], c2 a2 (h c/λ - eg2[T1] + ep2)^2/(Exp[ep2/(k T)] - 1), 0] +
    If[h c/λ - ep1 > eg1[T1], c1 a1 (h c/λ - eg1[T1] - ep1)^2/(-Exp[-ep1/(k T)] + 1), 0] +
    If[h c/λ - ep1 > eg2[T1], c1 a2 (h c/λ - eg2[T1] - ep1)^2/(-Exp[-ep1/(k T)] + 1), 0] +
    If[h c/λ - ep2 > eg1[T1], c2 a1 (h c/λ - eg1[T1] - ep2)^2/(-Exp[-ep2/(k T)] + 1), 0] +
    If[h c/λ - ep2 > eg2[T1], c2 a2 (h c/λ - eg2[T1] - ep2)^2/(-Exp[-ep2/(k T)] + 1), 0] +
    If[h c/λ > egd, ad (h c/λ - egd)^2, 0]) /. T1 → T;
```

Define the derivative of α**[T,**λ**]** with respect to temperature.

```
t1 = D[α[T1, λ1], T1];
dαdT[T_, λ_] := t1 /. {T1 → T, λ1 → λ}
```

Plot α as a Function of Wavelength for 300 K and 77 K

Plot α**[T,**λ**]** as a function of wavelength for 77 K and 300 K. The upper curve in the following figure is the one for 300 K.

```
<< Graphics`Graphics`
```

```
LogPlot[{10^4 α[T, λ] /. vars /. T → 77., 10^4 α[T, λ] /. vars /. T → 300.},
  {λ, 400., 1000.}, Frame → True,
  PlotRange → {{400., 1000.}, {10., 100000.}},
  FrameLabel → {"Wavelength (nm)", "Absorption constant (1/cm)"}];
```

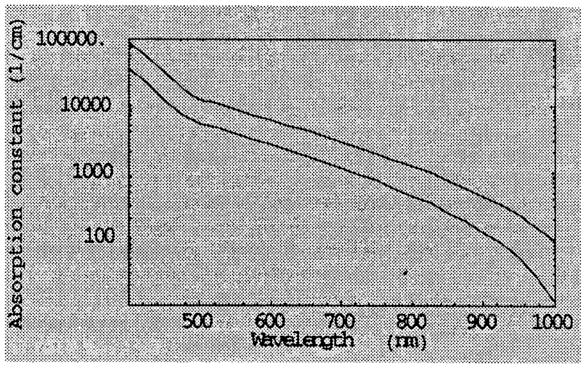

Perform Calculations Over Wavelength Band

The quantities that we calculate are an average over the wavelength band from 400 nm to 1000 nm. In these calculations, we assume that the photon flux is independent of wavelength, which should be satisfactory for our purposes here.

Plot relative quantum efficiency as a function of temperature.

```
Plot[1/600 NIntegrate[(1 - Exp[-α[T, λ] 2 t] /. vars), {λ, 400., 1000.}],
  {T, 20., 300}, Frame → True,
  FrameLabel → {"Temperature (K)", "Relative Quantum Efficiency"}];
```

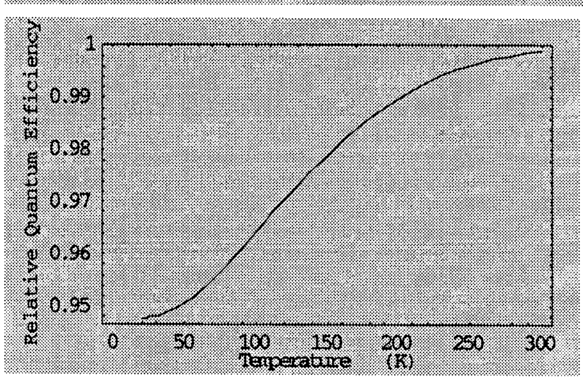

Calculate the derivative of the relative quantum efficiency at 72 K.

```
(2 t NIntegrate[dαdT[T, λ] Exp[-α[T, λ] 2 t] /. vars /. T → 72.,
    {λ, 400., 1000.}] /. vars) /
 (NIntegrate[(1 - Exp[-α[T, λ] 2 t] /. vars /. T → 72.), {λ, 400., 1000.}])
```

```
0.000292832
```

Plot the derivative of the fractional quantum efficiency as a function of temperature.

```
Plot[(2 t NIntegrate[
      (dαdT[T, λ] Exp[-α[T, λ] 2t]) /. vars, {λ, 400., 1000.}] /. vars) /
   (NIntegrate[(1 - Exp[-α[T, T] 2 λ] /. vars), {λ, 400., 1000.}] /. vars),
  {T, 20., 300.}, Frame → True,
  FrameLabel → {"Temperature (K)", "dE/dT"}];
```

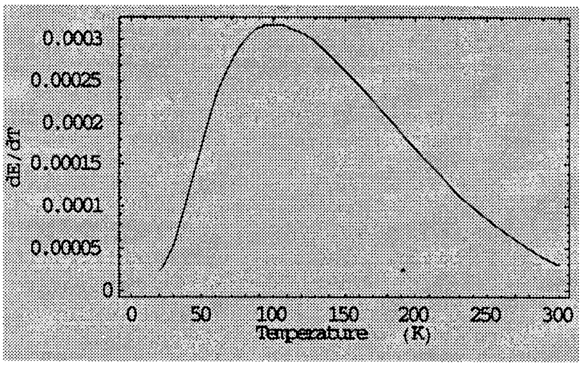
0.0003
0.00025
0.0002
0.00015
0.0001
0.00005
0
dE/dT
0
50
100
150
200
250
300
Temperature (K)